Published August 1, 2016

BLOC-1 and BLOC-3 regulate VAMP7 cycling to and from melanosomes via distinct tubular transport carriers

Megan K. Dennis,[1,2,3] Cédric Delevoye,[4,5,6] Amanda Acosta-Ruiz,[1,2,3] Ilse Hurbain,[4,5,6] Maryse Romao,[4,5,6] Geoffrey G. Hesketh,[7] Philip S. Goff,[8] Elena V. Sviderskaya,[8] Dorothy C. Bennett,[8] J. Paul Luzio,[7] Thierry Galli,[9] David J. Owen,[7] Graça Raposo,[4,5,6] and Michael S. Marks[1,2,3]

[1]Department of Pathology and Laboratory Medicine, Children's Hospital of Philadelphia Research Institute, Philadelphia, PA 19104
[2]Department of Pathology and Laboratory Medicine and [3]Department of Physiology, Perelman School of Medicine, University of Pennsylvania, Philadelphia, PA 19104
[4]Institut Curie, PSL Research University, Centre National de la Recherche Scientifique, UMR144, [5]Structure and Membrane Compartments, Institut Curie, and [6]Cell and Tissue Imaging Facility (PICT-IBiSA), 75005 Paris, France
[7]Cambridge Institute for Medical Research, University of Cambridge, Cambridge CB2 OXY, England, UK
[8]Cell Biology and Genetics Research Centre, St. George's, University of London, London SW17 ORE, England, UK
[9]University Paris Diderot, Sorbonne Paris Cité, Institut Jacques Monod, CNRS UMR 7592, Membrane Traffic in Health and Disease, INSERM ERL U950, 75013 Paris, France

Endomembrane organelle maturation requires cargo delivery via fusion with membrane transport intermediates and recycling of fusion factors to their sites of origin. Melanosomes and other lysosome-related organelles obtain cargoes from early endosomes, but the fusion machinery involved and its recycling pathway are unknown. Here, we show that the v-SNARE VAMP7 mediates fusion of melanosomes with tubular transport carriers that also carry the cargo protein TYRP1 and that require BLOC-1 for their formation. Using live-cell imaging, we identify a pathway for VAMP7 recycling from melanosomes that employs distinct tubular carriers. The recycling carriers also harbor the VAMP7-binding scaffold protein VARP and the tissue-restricted Rab GTPase RAB38. Recycling carrier formation is dependent on the RAB38 exchange factor BLOC-3. Our data suggest that VAMP7 mediates fusion of BLOC-1–dependent transport carriers with melanosomes, illuminate SNARE recycling from melanosomes as a critical BLOC-3–dependent step, and likely explain the distinct hypopigmentation phenotypes associated with BLOC-1 and BLOC-3 deficiency in Hermansky–Pudlak syndrome variants.

Introduction

Secretory and endolysosomal organelles mature by the membrane transport–dependent delivery of cargoes and removal of excess material. Cargo delivery requires sorting from a source compartment into nascent transport carriers; motility of the carriers toward the target organelle; and tethering, docking, and fusion of the carriers with the maturing target (Bonifacino and Glick, 2004). Cargo removal exploits similar processes and is particularly important to recycle fusion machinery components to the source membrane for additional rounds of cargo delivery (Bonifacino and Glick, 2004; Jahn and Scheller, 2006). Although the molecular details underlying fusion machinery cycling among early secretory pathway organelles are well developed (Cai et al., 2007; Barlowe and Miller, 2013), fusion machinery trafficking in the endosomal system is poorly characterized. This cycling is particularly critical during the maturation of lysosome-related organelles (LROs), which comprise specialized cell type–specific organelles that derive from the endosomal system but support distinct physiological functions in metazoans (Marks et al., 2013). LRO biogenesis requires dedicated and nonredundant pathways for content delivery; a similar dedicated pathway for content removal has not been described.

The importance of dedicated trafficking pathways in LRO biogenesis is underscored by Hermansky–Pudlak syndrome (HPS), a group of genetic diseases in which some LROs fail to mature properly with consequently impaired vision, skin and hair pigmentation, blood clotting, and often lung function (Wei, 2006; Wei and Li, 2013). HPS results from mutations in any of at least 10 genes that encode subunits of four cytoplasmic multisubunit protein complexes: adaptor protein-3 (AP-3) and biogenesis of lysosome-related organelles complex (BLOC) 1, 2,

Correspondence to Michael S. Marks: marksm@mail.med.upenn.edu

Abbreviations used: BF, bright field; FM, fluorescence microscopy; fps, frames per second; GEF, guanine nucleotide exchange factor; HPS, Hermansky–Pudlak syndrome; LRO, lysosome-related organelle; RPE, retinal pigment epithelia; WT, wild type.

© 2016 Dennis et al. This article is distributed under the terms of an Attribution–Noncommercial–Share Alike–No Mirror Sites license for the first six months after the publication date (see http://www.rupress.org/terms). After six months it is available under a Creative Commons License (Attribution–Noncommercial–Share Alike 3.0 Unported license, as described at http://creativecommons.org/licenses/by-nc-sa/3.0/).

Supplemental Material can be found at:
/content/suppl/2016/07/22/jcb.201605090.DC1.html

The Rockefeller University Press $30.00
J. Cell Biol. Vol. 214 No. 3 293–308
www.jcb.org/cgi/doi/10.1083/jcb.201605090

THE JOURNAL OF CELL BIOLOGY

Downloaded from on October 24, 2016

Published August 1, 2016

and 3 (Dell'Angelica, 2004; Di Pietro and Dell'Angelica, 2005). These complexes are thought to regulate membrane trafficking during LRO biogenesis, as best characterized in the maturation of melanosomes, the LROs in which melanins are synthesized and stored in pigment cells of the hair, skin, and eyes (Sitaram and Marks, 2012). AP-3, BLOC-1, and BLOC-2 affect the delivery of melanogenic enzymes, transporters, and accessory proteins from early endosomes to nonpigmented melanosome precursors via two pathways. One pathway requires BLOC-1 (Setty et al., 2007, 2008; Cullinane et al., 2011; Sitaram et al., 2012), together with the microtubule motor KIF13A and actin remodeling factors (Delevoye et al., 2009, 2016), for melanosome cargoes to exit endosomes into tubular transport carriers. BLOC-2 then targets these carriers specifically to melanosomes (Dennis et al., 2015). A second BLOC-1– and BLOC-2–independent pathway requires AP-3 for cargo sorting into melanosome-bound vesicles (Huizing et al., 2001; Theos et al., 2005; Setty et al., 2007, 2008), although AP-3 can also cooperate with BLOC-1 (Newell-Litwa et al., 2009; Sitaram et al., 2012). How BLOC-3 functions during melanosome biogenesis is not clear. BLOC-3 is a guanine nucleotide exchange factor (GEF) for the cell type–restricted Rab GTPases RAB32 and RAB38 (Gerondopoulos et al., 2012). BLOC-3 and both Rabs are implicated in the biogenesis of melanosomes and other LROs (Wasmeier et al., 2006; Lopes et al., 2007; Osanai et al., 2010; Bultema et al., 2012, 2014), but whether they function in pathways into or out of melanosomes is not known.

To deliver their contents to maturing melanosomes, endosome-derived transport carriers must fuse with the melanosome membrane. Membrane fusion within the endomembrane system is mediated by SNARE proteins (Chen and Scheller, 2001; Jahn and Scheller, 2006). Typically, engagement of v-SNAREs on transport carriers with cognate three-helix t-SNARE complexes on target membranes leads to assembly of stable four-helix bundles that destabilize the membrane and drive fusion (Domanska et al., 2010; Mohrmann et al., 2010). Several SNAREs have been implicated in melanosome biogenesis (Huang et al., 1999; Wade et al., 2001; Ghiani et al., 2010; Tamura et al., 2011; Yatsu et al., 2013; Jani et al., 2015), but among them, VAMP7 (also known as tetanus neurotoxin insensitive or TI-VAMP) is the only v-SNARE. VAMP7 facilitates fusion of late endosomes with lysosomes (Luzio et al., 2010) and with maturing secretory autophagosomes (Fader et al., 2009, 2012), as well as glycosylphosphatidylinositol-anchored protein delivery to the plasma membrane (Molino et al., 2015). An additional role for VAMP7 in melanosome maturation is suggested by its localization to melanosomes (Jani et al., 2015) and by the hypopigmentation (Jani et al., 2015) and mistrafficking of the melanosomal protein TYRP1 (Tamura et al., 2011) in VAMP7-depleted cells. Moreover, the VAMP7- and RAB32/38-interacting protein VARP is required for proper TYRP1 localization (Tamura et al., 2009) and must bind VAMP7 for this function (Tamura et al., 2011). However, it is not known whether the VAMP7 requirement is direct or in which pathway it participates. Additionally, although Hrb facilitates VAMP7 recycling from the plasma membrane after fusion with VAMP7-containing organelles (Pryor et al., 2008), a pathway for recycling VAMP7 from intracellular organelles has not been described in any cell system.

Here, we exploit quantitative live-cell imaging analyses of VAMP7 dynamics in immortalized melanocytes from mouse HPS models. We show that VAMP7 is a BLOC-1–dependent cargo that likely functions as the v-SNARE during fusion of tubular transport intermediates with maturing melanosomes. Importantly, we also describe a distinct tubular pathway to retrieve VAMP7 from melanosomes after cargo delivery and show that this pathway requires BLOC-3. Our data provide the first evidence of SNARE recycling from a LRO, provide new insights into SNARE recycling in the late endosomal system in mammalian cells, and identify a novel membrane trafficking step in melanocytes that is regulated by BLOC-3.

Results

VAMP7 localizes to melanosomes and is required for melanosome cargo trafficking and pigmentation

VAMP7 is thought to localize to melanosomes and to be required for melanogenesis (Tamura et al., 2011; Yatsu et al., 2013; Jani et al., 2015). We first confirmed the localization of VAMP7 in immortal mouse melanocytes derived from C57BL/6 mice (melan-Ink4a [wild type {WT}] or melan-a; Bennett et al., 1987; Sviderskaya et al., 2002). When expressed in WT mouse melanocytes, EGFP-tagged VAMP7 (GFP-VAMP7) localized by fluorescence microscopy (FM) extensively to pigmented melanosomes in the cell periphery (82 ± 6%; $n = 13$ cells), and marked pigment granules more predictably ($P < 0.0001$) than the melanosomal cargo protein TYRP1 (65 ± 12% overlap; $n = 13$ cells) with which VAMP7 partially overlapped (Fig. 1, a–c). Immuno-EM using immunogold labeling on ultrathin cryosections of transfected WT melan-a cells confirmed that GFP-VAMP7 localizes to the limiting membrane of pigmented melanosomes and adjacent vesicular structures (Fig. 1 d, arrows). To identify the specific cargo trafficking defect in VAMP7-deficient cells, we depleted VAMP7 in human MNT-1 melanoma cells by siRNA-mediated knockdown (Fig. 1 e). Consistent with previous observations by bright-field (BF) microscopy (Yatsu et al., 2013; Jani et al., 2015), analysis by standard EM showed that VAMP7-depleted MNT-1 cells harbored fewer fully pigmented stage IV melanosomes and less overall pigmentation than control siRNA-treated MNT-1 cells (Fig. 1, f–h). Quantification of immunogold labeling by immuno-EM showed that whereas TYRP1 localizes predominantly to melanosomes in control siRNA-treated MNT-1 cells, a large cohort is mislocalized to tubulovesicular endosomes adjacent to melanosomes in VAMP7-depleted cells (Fig. 1, i–k, arrowheads). These data support a role for VAMP7 in pigmentation by trafficking melanosomal cargoes such as TYRP1 from endosomes to maturing melanosomes.

VAMP7 traffics to melanosomes in BLOC-1–dependent tubular carriers

To determine whether VAMP7 traffics to melanosomes via BLOC-1–independent or –dependent pathways, we analyzed GFP-VAMP7 localization in BLOC-1–deficient (BLOC-$1^{-/-}$) melanocytes relative to melanosomal cargoes and the pan-early endosomal SNARE syntaxin 13 (STX13; also known as syntaxin 12) by FM. In melanocyte cell lines (melan-pa and melan-mu) from two different BLOC-$1^{-/-}$ mouse models (*pallid* and *muted*), GFP-VAMP7 was retained (79 ± 7% in melan-pa; $n = 53$ cells) in sorting and recycling endosomes, marked by expression of mCherry-STX13 (mCh-STX13; Fig. 2, a–e, arrowheads; and Fig. S1, f–i, arrowheads; compare to WT in Fig. S1, a–e, arrows) to an even higher extent ($P < 0.0001$) than the BLOC-1–dependent melanosome cargo TYRP1 (66 ± 14%

Downloaded from on October 24, 2016

Published August 1, 2016

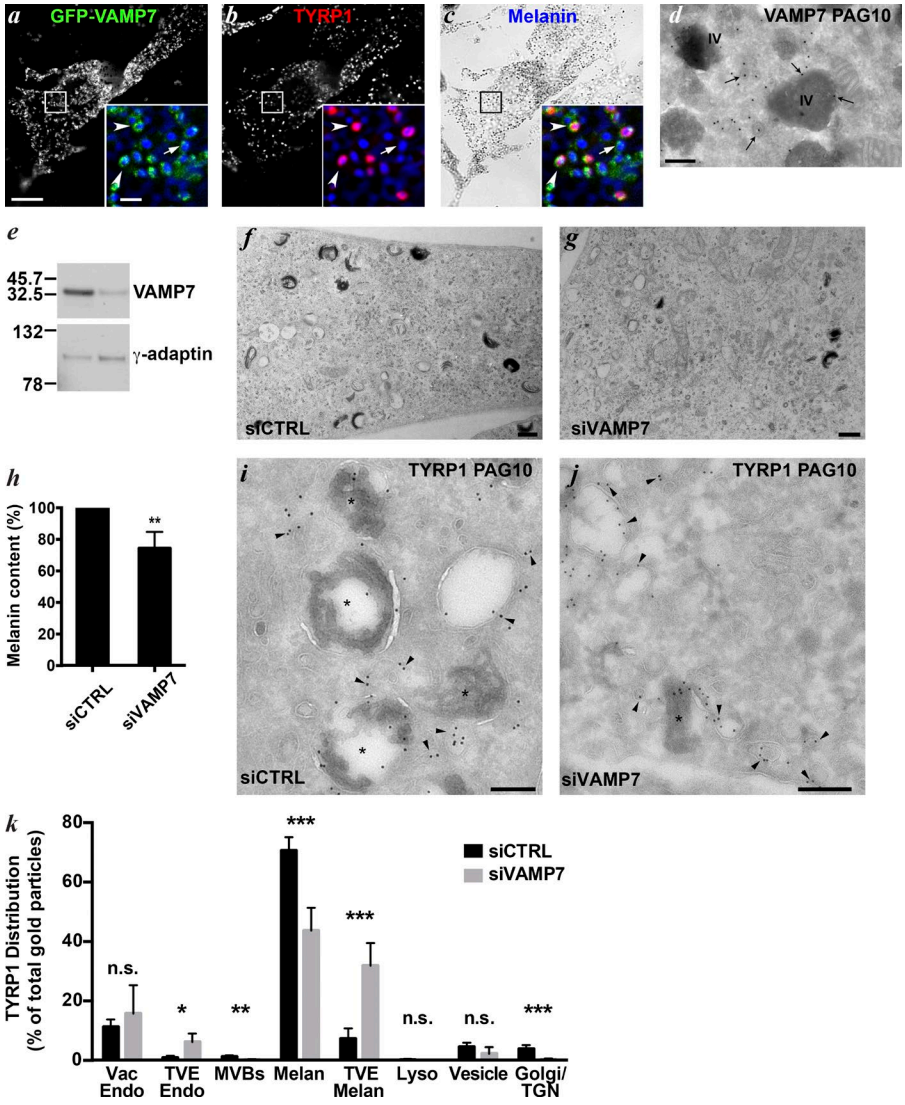

Figure 1. **VAMP7 localizes to melanosomes and is required for pigmentation and cargo trafficking.** (a–c) WT melan-Ink4a melanocytes transiently expressing GFP-VAMP7 (green) were fixed and labeled for TYRP1 (red) and analyzed by deconvolution immuno-FM. Bar, 10 µm. BF (melanin) image in c is pseudocolored blue in insets. Insets of boxed regions are magnified five times; bar, 1 µm. Melanosomes labeled by both VAMP7 and TYRP1 (arrowheads) or VAMP7 only (arrow) are indicated. (d) Ultrathin cryosection of WT melan-a melanocytes transfected with GFP-VAMP7 and labeled for VAMP7 with 10 nm protein A gold (PAG10). Arrows show GFP-VAMP7 on stage IV melanosomes (IV) and adjacent vesicles. Bar, 200 nm. (e–k) MNT-1 melanoma cells treated with control (siCTRL) or VAMP7-specific siRNA (siVAMP7) were analyzed 5 d later. (e) Whole-cell lysates fractionated by SDS-PAGE were immunoblotted for VAMP7 or the AP-1 subunit γ-adaptin as a control. Relevant bands and positions of nearby molecular weight markers are shown. (f and g) Thin sections of fixed cells in epon were analyzed by conventional EM. Bars, 500 nm. (h) Melanin content in cell lysates was assayed by spectrophotometry. Data are normalized to siCTRL and represent mean ± SD from at least three experiments. (i and j) Ultrathin cryosections of fixed cells were labeled for TYRP1 with PAG10. Asterisks show pigmented melanosomes, and arrowheads show TYRP1 labeling on melanosomal membrane or closely adjacent vesicular structures. Bars, 200 nm. (k) Quantification of TYRP1 localization in siCTRL and siVAMP7 cells (mean ± SD from three measurements). Golgi/TGN, Golgi and trans-Golgi network; Lyso, lysosomes; Melan, melanosomes; MVBs, multivesicular bodies; TVE endo, tubulovesicular endosomes associated with endosomes; TVE Melan, tubulovesicular endosomes associated with melanosomes; Vac Endo, vacuolar endosomes; Vesicle, other vesicular structures. *, $P < 0.05$; **, $P < 0.01$; ***, $P < 0.005$; n.s., no significant difference.

in melan-pa; Setty et al., 2007). Melanosomal localization of GFP-VAMP7 was restored by stable expression of the missing Pallidin or Muted subunits (melan-pa:MycPa or BLOC-1^R and melan-mu:MuHA rescue) before GFP-VAMP7 expression (Fig. 2, f–j; and Fig. S1, j–m). VAMP7 mislocalization in BLOC-$1^{-/-}$ cells does not reflect global VAMP mistrafficking, as localization of VAMP2, VAMP4, and VAMP8 was unaffected in BLOC-$1^{-/-}$ cells compared with WT melanocytes (Fig. 2, k–p). Together, these data suggest that VAMP7 is a BLOC-1–dependent melanosome cargo.

To test whether VAMP7 is targeted to melanosomes in BLOC-1–dependent tubular carriers, we exploited the endosomal retention of VAMP7 in BLOC-$1^{-/-}$ cells. BLOC-1–dependent cargo trafficking in real time is difficult to study in WT melanocytes, as cargoes such as TYRP1 are localized largely to mature pigmented melanosomes at steady state (Orlow et al., 1993; Vijayasaradhi et al., 1995; Setty et al., 2007) and thus the fraction of TYRP1 actively trafficking to melanosomes is small and difficult to detect. Because stable reexpression of Pallidin in BLOC-$1^{-/-}$ melan-pa melanocytes restores GFP-VAMP7 localization to melanosomes, we surmised that analysis of melan-pa cells soon after transient expression of Pallidin might allow us to visualize early BLOC-1–dependent transport events. We thus cotransfected melan-pa cells with myc-Pallidin, GFP-VAMP7, and mCh-STX13 and analyzed fixed cells by FM at various times after transfection (Fig. 2, q–v). We observed a time-dependent decrease in the extensive overlap between GFP-VAMP7 and mCh-STX13 in endosomes (arrowheads) and a concomitant increase in GFP-VAMP7–labeled structures that lacked mCh-STX13 (arrows). This GFP-VAMP7 redistribution required BLOC-1 function, as it was not observed upon cotransfection of Pallidin-deficient melan-pa cells with an excess of the Muted subunit (Fig. 2, q, u, and v; and Fig. 3, a–d and m–p), which does not restore BLOC-1 expression (Setty et al., 2007). The GFP-VAMP7–containing, mCh-STX13–negative structures were newly generated maturing melanosomes that had not yet accumulated pigment, because they contained TYRP1 (Fig. 3, e–l, arrows) and the early-stage melanosome marker PMEL (Fig. 3, q–t, arrows).

Like the early endosomes from which they derive, the BLOC-1–dependent tubular carriers through which cargoes such as TYRP1 are transferred to melanosomes, but not melanosomes themselves, were labeled by GFP- or mCh-STX13 (Setty et al., 2007; Delevoye et al., 2009, 2016; Dennis et al., 2015). To test whether VAMP7 is transported through these carriers, we analyzed melan-pa melanocytes 20 h after cotransfection with myc-Pallidin, GFP-VAMP7, and mCh-STX13.

Downloaded from on October 24, 2016

Published August 1, 2016

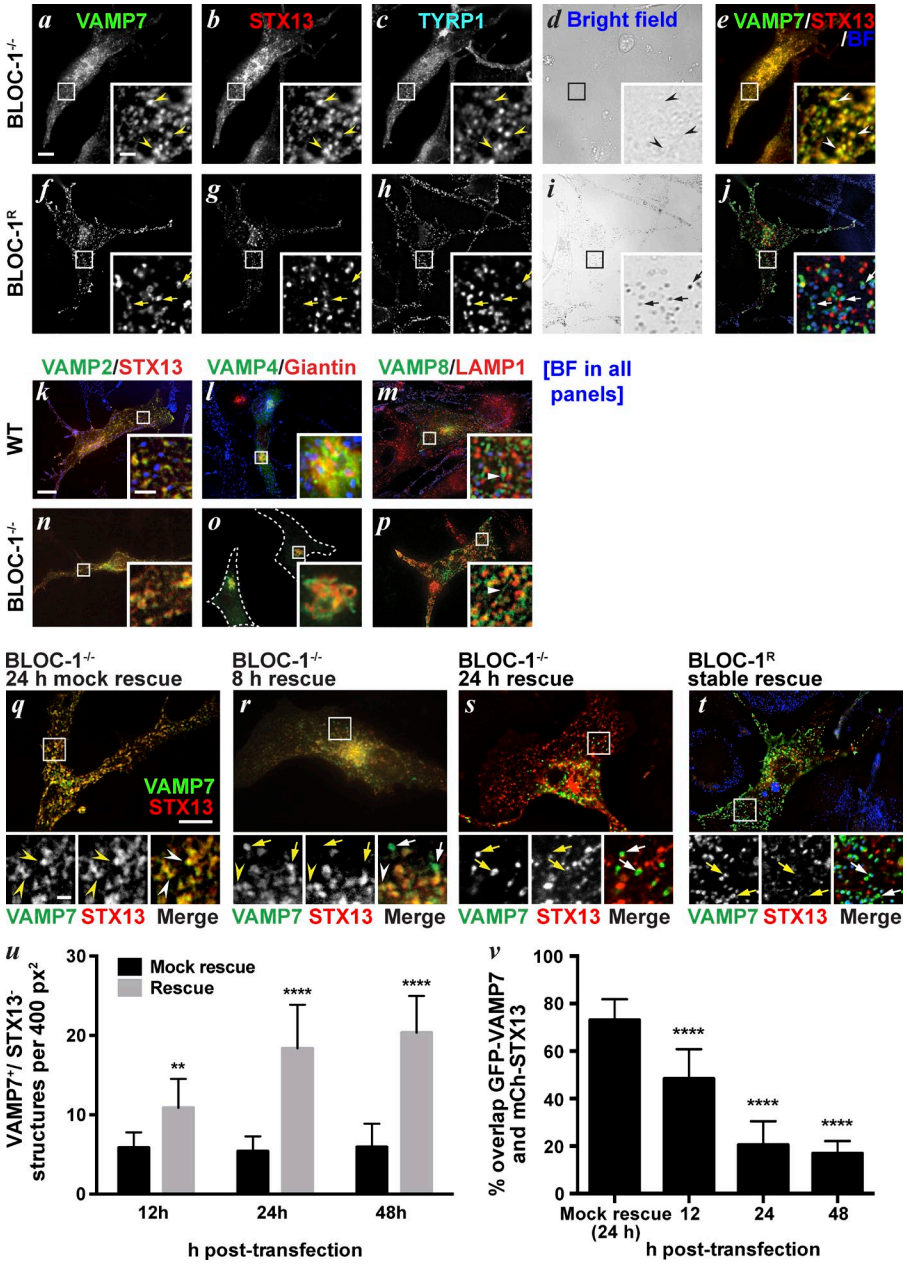

Figure 2. **VAMP7 is a BLOC-1 cargo.** (a–j) BLOC-1–deficient melan-pa (BLOC-1$^{-/-}$; a–e) or "rescued" melan-pa cells stably expressing myc-Pallidin (BLOC-1^{R}; f–j) and transiently expressing GFP-VAMP7 (green) and mCh-STX13 (red) were fixed and labeled for TYRP1 (cyan) and analyzed by deconvolution immuno-FM. Arrowheads show GFP-VAMP7 and TYRP1 retained in mCh-STX13–positive endosomes, and arrows show melanosomes with GFP-VAMP7 and TYRP1 but lacking mCh-STX13. Insets of boxed regions are magnified five times. (k–m) WT melan-Ink4a (n–p) and BLOC-1–deficient melan-pa (BLOC-1$^{-/-}$) transiently expressing GFP-VAMP2 (green) and mCh-STX13 (red, k and n), VAMP4-HA (green, l and o), or GFP-VAMP8 (green, m and p) were fixed, labeled for HA (green) and Giantin (red, l and o) or for LAMP1 (red, m and p), and analyzed by deconvolution immuno-FM. Merged images are shown with BF images pseudocolored blue. Dashed line in o indicates cell borders. Insets are boxed regions magnified six times. (q–v) BLOC-1$^{-/-}$ melan-pa melanocytes transiently transfected with GFP-VAMP7 (green), mCh-STX13 (red), and either myc-Pallidin ("rescue") or myc-Muted ("mock rescue") for indicated times. Arrowheads show GFP-VAMP7 retained in mCh-STX13 endosomes; and arrows point to GFP-VAMP7 in melanosome precursors. Note that pigmentation is not detected until ∼72 h after transfection with myc-Pallidin. Insets are boxed regions magnified 3.5 times. (u) Quantification (mean ± SD from 15 regions of at least nine cells per time point representing three independent experiments) of GFP-VAMP7–labeled structures that lack mCh-STX13 in rescue and mock rescue cells at 12, 24, and 48 h after transfection. (v) Area (mean ± SD from at least 15 cells per time point representing four independent experiments) of overlap between GFP-VAMP7 and mCh-STX13 in the periphery of mock rescue and rescue cells quantified at 12, 24, and 48 h after transfection. **, P < 0.01; ****, P < 0.0001. BF images in d, l, and k–t are pseudocolored blue in merge. Bars: (a–t) 10 µm; (insets) 2 µm.

In such transiently rescued BLOC-1$^{-/-}$ cells, unlike in WT or stably rescued BLOC-1^{R} cells in which mCh-STX13 is largely segregated from GFP-VAMP7 and TYRP1-GFP (Fig. 4, a–f; Fig. S2, a and b; and Videos 1 and 2), tubules emerging from mCh-STX13-labeled endosomes that contain both mCh-STX13 and either GFP-VAMP7 (Fig. 4, g–j, arrows; and Video 3) or TYRP1-GFP (Fig. 4, k–n, arrows; and Video 4) were readily visualized. In contrast, in control mock rescued cells expressing Muted-HA, STX13 tubule formation was dramatically impaired (as quantified in Delevoye et al., 2016) and GFP-VAMP7 was retained in mCh-STX13–positive vacuolar endosomes (Fig. S2, c–f, arrowheads; and Video 5). These data provide direct evidence that both melanosomal cargoes and VAMP7 traffic from early endosomes to melanosomes via STX13-containing tubules. Given the role of VAMP7 in TYRP1 delivery to melanosomes (Fig. 1), we conclude that VAMP7 likely functions in fusion of BLOC-1–dependent endosomal carriers with maturing melanosomes.

VAMP7 recycles from melanosomes in tubular carriers that lack STX13

If VAMP7 functions as a canonical v-SNARE in the fusion of endosomal transport carriers with maturing melanosomes, it must be retrieved from melanosomes for use in future rounds of cargo delivery. Consistently, we observed GFP-VAMP7–labeled structures emanating from pigmented melanosomes by live-cell fluorescence and BF microscopy of WT melanocytes (Figs. 5, a–c; Fig. S2 i; and Video 6). The GFP-VAMP7–labeled tubules (arrows) were distinct from the anterograde mCh-STX13–labeled tubules (arrowheads) that deliver cargo to melanosomes, as assessed by dual-color imaging (Fig. 5, d–g; and Video 1). This subpopulation of GFP-VAMP7–positive, melanosome–derived tubules were independent of, and shorter in length and less stable than, those labeled solely by mCh-STX13 (P < 0.0001, n = 50 tubules each; Fig. S2, g and h). The GFP-VAMP7 tubules that exit melanosomes did not contain detectable mRFP-tagged OCA2 or TYRP1 (Fig. 5, h–j; Fig. S2, k–n; and

Downloaded from on October 24, 2016

Published August 1, 2016

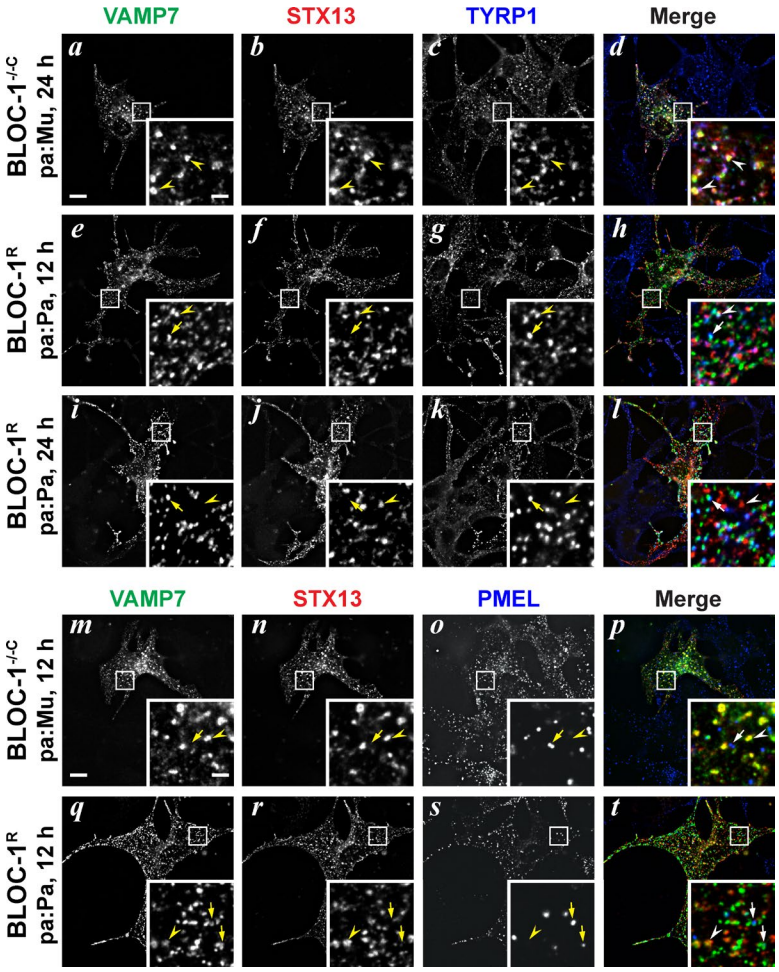

Figure 3. **VAMP7 traffics with TYRP1 to maturing melanosomes upon BLOC-1 rescue.** (a–t) BLOC-1$^{-/-}$ (melan-pa) cells transiently transfected with GFP-VAMP7 (green), mCh-STX13 (red), and either myc-Pallidin (BLOC-1^{R}) or myc-Muted (BLOC-1$^{-/-C}$) were fixed 12 or 24 h after transfection. Cells were then immunolabeled for TYRP1 (blue, a–l) or PMEL (blue, m–t) and analyzed by deconvolution immuno-FM. Arrowheads show GFP-VAMP7 and TYRP1 (a–l) or GFP-VAMP7 alone (m–t) retained in mCh-STX13–labeled endosomes, and arrows point to GFP-VAMP7 and either TYRP1 (a–l) or PMEL (m–t) colabeled in melanosomal precursors that lack mCh-STX13. Insets are boxed regions magnified five times. Bars: (main) 10 µm; (insets) 2 µm.

Videos 7 and 8), suggesting that they were selective for cargo destined for removal from melanosomes. Thus, GFP-VAMP7 labels membrane transport carriers that emerge from maturing melanosomes with characteristics of those that recycle SNAREs (Bonifacino and Glick, 2004; Jahn and Scheller, 2006).

VARP is associated with VAMP7 recycling tubules and is recruited to melanosomes by RAB38 and VAMP7

VAMP7 contains an autoinhibitory longin domain that can block VAMP7 interactions with cognate SNAREs (Martinez-Arca et al., 2003). The scaffolding protein VARP binds both the longin and SNARE domains of VAMP7 (Burgo et al., 2009), keeping VAMP7 in an autoinhibited conformation and impeding its fusogenic activity (Schäfer et al., 2012). VARP was proposed to support melanosome biogenesis via its ability to bind to VAMP7 (Tamura et al., 2009) and to mediate endosomal recycling in non-LRO–containing cells (Hesketh et al., 2014). Thus, we tested whether VARP associates with VAMP7 retrieved from melanosomes. When expressed in WT melanocytes, GFP- or HA-tagged VARP localized in part (30% ± 6%) to puncta adjacent to melanosomes in the cell periphery (Fig. 6, a–f), and in part (70% ± 6%) to endosomal structures, as in nonmelanocytic cells (Hesketh et al., 2014), that predominated in the perinuclear region (Fig. 6, g–i). By spinning-disk microscopy analysis of WT melanocytes, VARP-GFP was detected on nearly all mCh-VAMP7 tubulovesicular structures (arrows) that exited from melanosomes (arrowhead) in the cell periphery (Figs. 6, j–l; Fig. S3 a; and Video 9). Like the VAMP7-labeled tubules, VARP-GFP–labeled tubules were not enriched for the melanosomal cargoes TYRP-mRFP or mRFP-OCA2 (Figs. 6, m–o; Fig. S3, b and e–h; and Videos 10 and 11). These results place VARP on the VAMP7-containing tubules that exit melanosomes, where VARP might stabilize VAMP7 in a nonfusogenic state. VARP-GFP–labeled tubules also extended from mCh-STX13–labeled endosomes in the perinuclear region (Fig. 6, p–r; Fig. S3 c; and Video 12), but they were distinct from the STX13-labeled tubules that traffic cargo to melanosomes (Fig. 6, s–u; Fig. S3 d; and Video 12) and likely represent carriers that recycle cargoes such as GLUT-1 to the cell surface (Hesketh et al., 2014) or that mediate retrograde endosome to TGN trafficking (Wassmer et al., 2009).

In addition to VAMP7, VARP binds to RAB32/38 and the VPS29/35 subunits of the retromer complex via distinct sites (Zhang et al., 2006; Wang et al., 2008; Burgo et al., 2009; Tamura et al., 2009; Hesketh et al., 2014; McGough et al., 2014) and functions as a RAB21 GEF (Zhang et al., 2006). In nonmelanocytic cells, retromer binding is required to recruit VARP to endosome-derived tubules, and both retromer and VARP participate in GLUT-1 trafficking to the cell surface (Hesketh et al., 2014; McGough et al., 2014). In melanocytes, TYRP1 localization to melanosomes requires both retromer (McGough et al., 2014) and VARP binding to VAMP7 and RAB32/38, but not RAB21 GEF activity (Tamura et al., 2011). Like VAMP7, RAB38 and RAB32 localize in part to melanosomes (Wasmeier et al., 2006; Bultema et al., 2012; Gerondopoulos et al., 2012).

Downloaded from on October 24, 2016

Published August 1, 2016

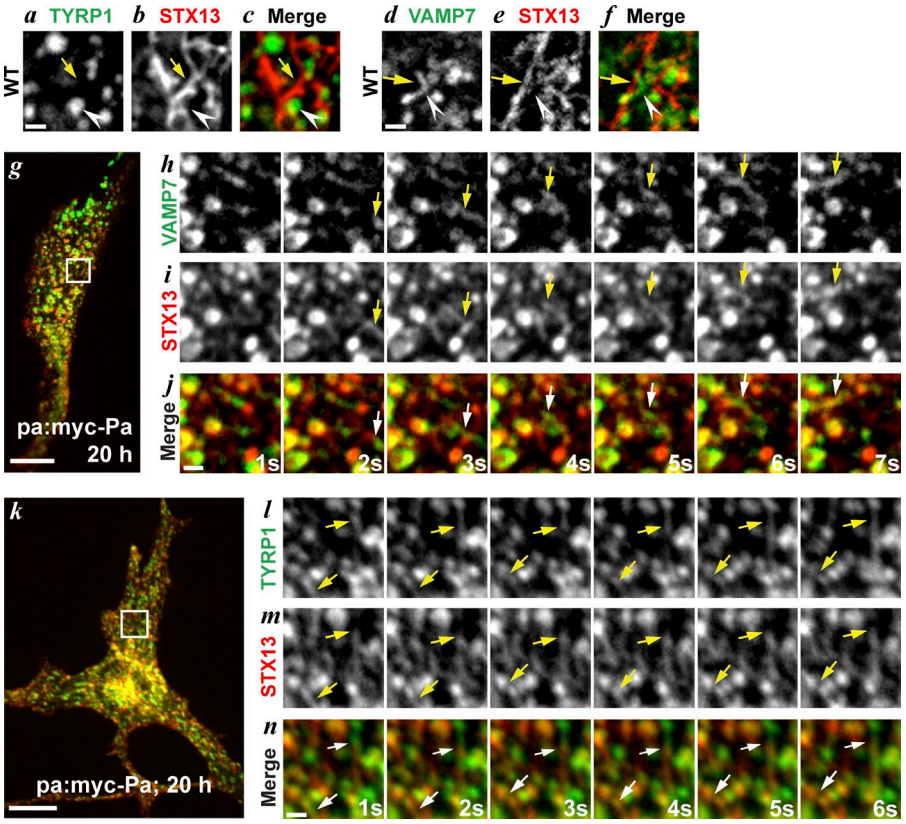

Figure 4. **VAMP7 and TYRP1 traffic to melanosomes in BLOC-1–dependent membrane tubules.** (a–f) WT melan-Ink4a cells transiently transfected with mCh-STX13 (red) and either TYRP1-GFP (green, a–c; cell shown in Fig. S2 a) or GFP-VAMP7 (green; d-f; cell shown in Figs. 5 d and S2 b) were analyzed 24 h later by spinning-disk confocal microscopy at 1 fps. Regions from a single frame are shown. Arrows, mCh-STX13-labeled endosomal tubules; arrowheads, TYRP1-GFP-labeled melanosome (a–c) or GFP-VAMP7-labeled tubule (d-f). Note that tubular mCh-STX13–labeled endosomes in live-cell analyses appear punctate upon fixation (e.g., Fig. 2, g, s, and t). Bar, 1 µm. (g–n) melan-pa melanocytes were transiently transfected with myc-Pallidin, mCh-STX13 and either GFP-VAMP7 (g–j) or TYRP1-GFP (k-n) and analyzed 20 h later by spinning-disk confocal microscopy at ∼1 fps. (g and k) Single frames of representative cells showing overlap of mCh-STX13 with GFP-VAMP7 (g) or TYRP1-GFP (k). Bars, 10 µm. Image sequences from the boxed regions in g and k are magnified five times in h–j and l–n, respectively. Arrows show mCh-STX13–labeled tubules containing GFP-VAMP7 (h–j) or TYRP1-GFP (l–n). Elapsed time (in seconds) is indicated at the lower right. Bars, 1 µm.

Indeed, GFP-RAB38 overlapped by FM with VARP-HA on puncta adjacent to melanosomes (Fig. 7, a–h) and, like VARP, GFP-RAB38 was detected on mCh-VAMP7–containing tubules that exit melanosomes (Fig. 7, i–l; and Video 13). Therefore, we investigated the requirement for VAMP7, RAB32/38, and retromer in recruiting VARP to melanosomes by exploiting VARP site-directed mutants in which binding to each partner is impaired (Hesketh et al., 2014). We expressed GFP-tagged full-length VARP or site-directed mutants in WT melanocytes and quantified GFP-positive puncta that associated with pigmented melanosomes (arrowheads) or with mCh-STX13–labeled endosomes (Fig. 8, a–g, arrows). Mutagenesis of either the VAMP7 or the RAB32/38 binding site resulted in decreased VARP localization to melanosomes by 57% ± 18% or 60% ± 19%, respectively, and loss of both binding sites led to a further reduction (87% ± 11% less than WT). However, as in nonpigmented cells (Hesketh et al., 2014), these mutations had no effect on VARP association with mCh-STX13–labeled early endosomes. In contrast, mutagenesis of the retromer binding site had no effect on melanosome localization but severely impaired the association of VARP with mCh-STX13 endosomes as in nonmelanocytic cells (Hesketh et al., 2014). Thus, VARP recruitment to pigmented melanosomes depends primarily on interactions with both VAMP7 and RAB32/38, with which it associates in retrograde transport carriers, and does not require binding to retromer.

BLOC-3 is required for RAB38 and VARP recruitment to melanosomes and facilitates formation of VAMP7 recycling tubules

BLOC-3, composed of HPS1 and HPS4 subunits that are defective in the majority of HPS patients (Seward and Gahl, 2013), is a GEF for RAB32 and RAB38 (Gerondopoulos et al., 2012), but the effects of BLOC-3 mutations on melanosome biogenesis are unclear and vary in different pigment cell types (Gardner et al., 1997; Nguyen et al., 2002; Richmond et al., 2005; Nguyen and Wei, 2007; Gerondopoulos et al., 2012). Like BLOC-3–deficient hair bulb melanocytes (Nguyen et al., 2002) and primary mouse melanocytes (Gardner et al., 1997), immortal BLOC-3–deficient melan-le (from HPS4-deficient *light ear* mice) and melan-ep (from HPS1-deficient *pale ear* mice) melanocytes harbor abundant pigmented melanosomes, some of which are unusually large (Fig. 9, c, l, and u; Fig. S4, g, k, and o; and Fig. S5, c, k, o, and w). The extent of TYRP1 localization to pigment granules in these cells was only slightly reduced relative to WT melanocytes (Fig. 9, a–h; and Fig. S4, a–d; 66% ± 6% of TYRP1 overlapped with pigment granules in WT melan-a cells, 56% ± 8% in melan-le; difference is not statistically significant); similarly, segregation of the lysosomal membrane protein LAMP2 from pigment granules was only slightly impaired (Fig. 9, a–h; and Fig. S4, a–d; 5% ± 3% of LAMP2 overlapped with pigment granules in WT melan-a cells, 14% ± 5% in melan-le; P = 0.003). These data indicate that BLOC-3 is not directly responsible for anterograde cargo trafficking to melanosomes or for gross melanosome segregation from the endolysosomal system. We thus tested whether BLOC-3 deficiency affected RAB38 and VARP localization and VAMP7 recycling. Consistent with BLOC-3 function as a RAB38 GEF, GFP-RAB38 in HPS4-deficient melan-le cells was largely diffuse and did not associate with pigment granules (Fig. 9, i–m). Accordingly, VARP localization to melanosomes was also substantially reduced in melan-le cells (Fig. 9, s–v). Stable reexpression of a WT HPS4 subunit in HPS4-deficient melan-le melanocytes, but not of excess WT HPS1, restored

Downloaded from on October 24, 2016

Published August 1, 2016

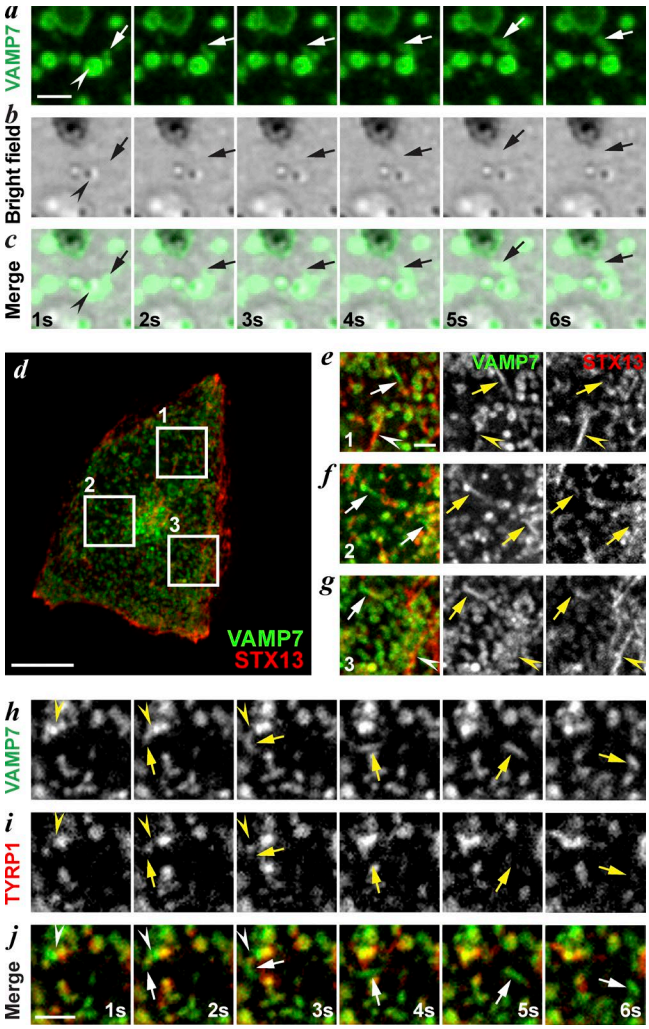

Figure 5. **GFP-VAMP7 exits melanosomes in STX13-independent tubules lacking TYRP1.** (a–f) WT melan-Ink4a melanocytes transiently transfected with GFP-VAMP7 alone (green, a–c) or with mCh-STX13 (red, d–g) or TYRP1-mRFP (red, h–j) were analyzed 24 h later by spinning-disk confocal microscopy at ∼1 fps. (a–c) Image sequence from a cell (shown in Fig. S2 i) expressing GFP-VAMP7 relative to melanosomes visualized by BF microscopy. Arrow shows a GFP-VAMP7 tubule, and the arrowhead points to a melanosome in the BF image. Bar, 2 µm. (d) Single frame from representative cell expressing GFP-VAMP7 and mCh-STX13. Bar, 10 µm. (e–g) Single frames from boxed regions in d with single channels and merged image. Arrows show tubules labeled by GFP-VAMP7 (green), and arrowheads show tubules labeled by mCh-STX13 (red). Bar, 1 µm. Insets are magnified two times from d. (h–j) Image sequence from a cell (shown in Fig. S2 j) expressing GFP-VAMP7 (green) and TYRP1-mRFP (red). A GFP-VAMP7–labeled tubule (arrow) emerges from a TYRP1-mRFP/GFP-VAMP7–labeled melanosome (arrowhead). Elapsed time is shown in seconds (s) at the bottom. Bar, 2 µm.

both RAB38 and VARP melanosomal localization to WT levels (Fig. 9, n–r and w–z; and Fig. S4, i–p). Similar data were obtained using HPS1-deficient melan-ep melanocytes and stable reexpression of "rescuing" HPS1 or "nonrescuing" HPS4 (Fig. S5, a–x). Thus, BLOC-3 activation is required for the recruitment and/or stabilization of RAB38 on/to melanosomes and for subsequent effective VARP recruitment.

To test whether BLOC-3 is required for VAMP7 recycling, we quantified the fission of GFP-VAMP7–containing tubules from melanosomes by live imaging of transiently transfected WT melanocytes, HPS4-deficient melan-le (le), or melan-le cells stably expressing either HPS1 (le:HPS1) or HPS4 (le:HPS4). As in WT melanocytes, the majority of GFP-VAMP7 (78% ± 9%, n = 23 cells; not significantly different from WT) localized to melanosomes in the periphery of melan-le cells (Fig. 9 j). However, whereas GFP-VAMP7–labeled tubules were frequently observed emanating from these structures in WT cells (Fig. 10, a and d; and Video 14), such tubules were rare in melan-le cells (Fig. 10, b and d). Restoration of BLOC-3 function by stable expression of HPS4 restored WT tubule frequency, whereas stable expression of HPS1 did not (Fig. 10, c and d). Thus, BLOC-3 regulates recycling of VAMP7 from melanosomes, most likely by recruiting RAB38 and consequently VARP to initiate and/or complete tubule formation.

Discussion

VAMP7 has been implicated in melanosome biogenesis (Tamura et al., 2011; Jani et al., 2015), but the pathways by which it is directed toward and recycled from melanosomes were unknown. Here, we show that VAMP7 functions during melanosome biogenesis primarily as a v-SNARE in BLOC-1–dependent tubular transport from endosomes to melanosomes and thereby promotes melanosomal delivery of BLOC-1–dependent cargoes such as TYRP1. Importantly, our analyses of VAMP7 dynamics revealed a previously undocumented SNARE retrieval pathway from maturing melanosomes. This pathway employs membrane tubules that emerge from melanosomes at sites enriched in RAB38 and VARP and that require the RAB32/38 GEF BLOC-3 for their formation. The resulting model (Fig. 10 e) has important implications for RAB32/38, BLOC-3, and VAMP7 function in the biogenesis of other LROs and in the etiology of the most common forms of HPS.

Cargoes are delivered to melanosomes by two distinct pathways that emerge from early endosomes: one that requires BLOC-1 and a second that is BLOC-1 independent (Sitaram and Marks, 2012). Our data using a novel transient rescue assay place VAMP7 on the BLOC-1–dependent pathway that also delivers melanosomal cargoes such as TYRP1 and OCA2. That VAMP7 is a cargo of the BLOC-1 pathway is consistent with the reduced VAMP7 levels in lysates of BLOC-1–deficient fibroblasts and 293T cells and in synaptic vesicle fractions of BLOC-1–deficient neurons (Salazar et al., 2006; Ryder et al., 2013). The altered TYRP1 distribution in cells depleted of VAMP7 indicates that VAMP7 likely functions as the main v-SNARE for cargo delivery in this pathway. Given that STX13 labels the BLOC-1–dependent transport intermediates (Dennis et al., 2015), this function for VAMP7 likely explains the reported requirement for VAMP7 in the accumulation of truncated STX13 on melanosomes (Jani et al., 2015). VAMP7 might similarly facilitate fusion of tubular intermediates between endosomes and lysosomes in cell types that lack LROs (Bright et al., 2005); formation of such tubules, like a subclass of recycling endosomes (Delevoye et al., 2016), might require BLOC-1 or the structurally related BORC (Pu et al., 2015).

v-SNAREs are thought to cycle back to their membrane of origin after cargo delivery to mediate additional rounds of cargo trafficking (Bonifacino and Glick, 2004; Jahn and Scheller, 2006). However, to our knowledge, the only described pathway for v-SNARE retrieval in the late endosomal system in mammalian cells is the Hrb-dependent recycling of VAMP7 from the plasma membrane after fusion with late endosomes (Pryor et al.,

Downloaded from on October 24, 2016

Published August 1, 2016

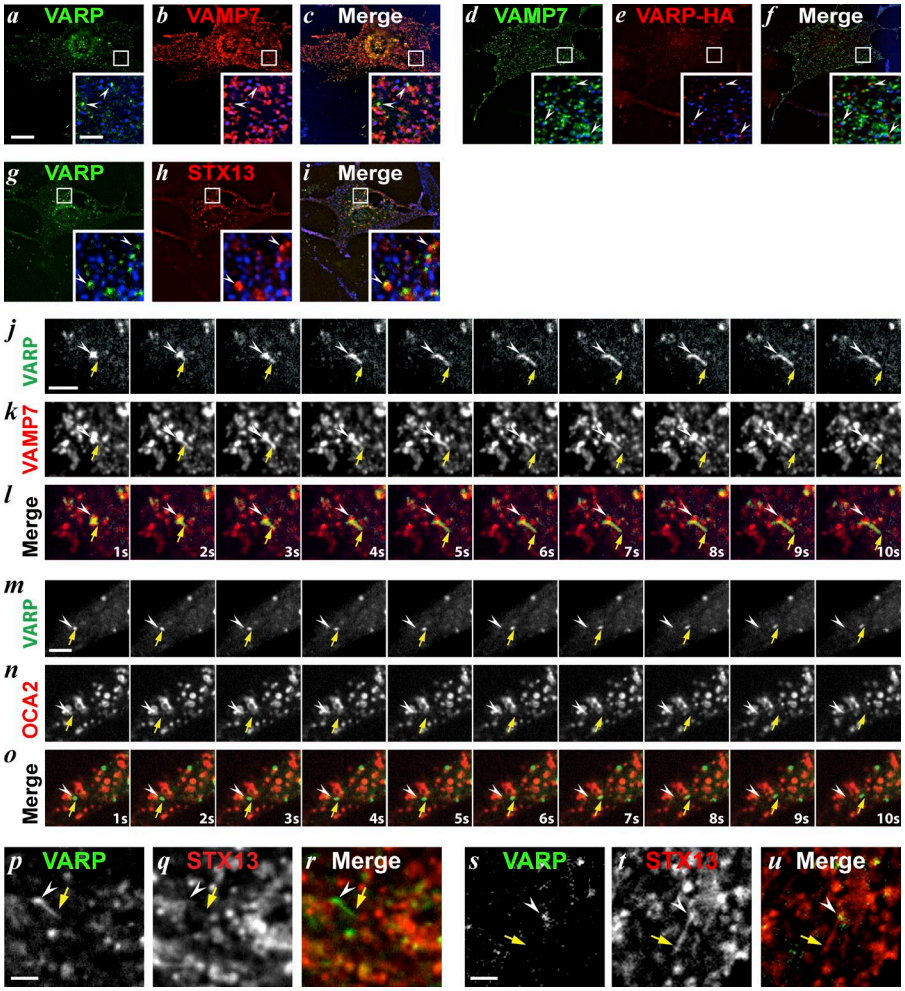

Figure 6. **A cohort of VARP localizes to melanosomes and accompanies GFP-VAMP7 on departing tubules.** (a–i) WT melan-Ink4a melanocytes transiently transfected with VARP-GFP and mCh-VAMP7 (a–c), GFP-VAMP7 and VARP-HA (d–f), or VARP-GFP and mCh-STX13 (g–i) were fixed 48 h later, labeled with anti-HA (d–f), and analyzed by deconvolution immuno-FM. BF images are pseudocolored blue and shown in merge and insets (boxes magnified five times). Arrowheads show VARP puncta adjacent to melanosomes (a–f) or to mCh-STX13–labeled endosomes (g–i). Bars: (main), 10 µm; (insets), 2 µm. (j–u) WT melan-Ink4a melanocytes transiently transfected with VARP-GFP and either mCh-VAMP7 (j-l; see Fig. S3 a), mRFP-OCA2 (m–o; see Fig. S3 b) or mCh-STX13 (p–u; see Fig. S3, c and d) were analyzed 48 h later by spinning-disk confocal microscopy at ∼1 fps. Elapsed time (in seconds) is indicated at lower right. (j–l) A VARP-GFP– and mCh-VAMP7–labeled tubule (arrow) extends from a melanosome (arrowhead). (m–o) A VARP-GFP–labeled vesicle (arrow) exits from an mRFP-OCA2–labeled melanosome (arrowhead). (p–r) A VARP-GFP tubule (arrow) departs from a mCh-STX13–labeled endosome (arrowhead). (s–u) A mCh-STX13 tubule (arrow) exits from a mCh-STX13/VARP-GFP double-labeled endosome (arrowhead). Bars, 2 µm.

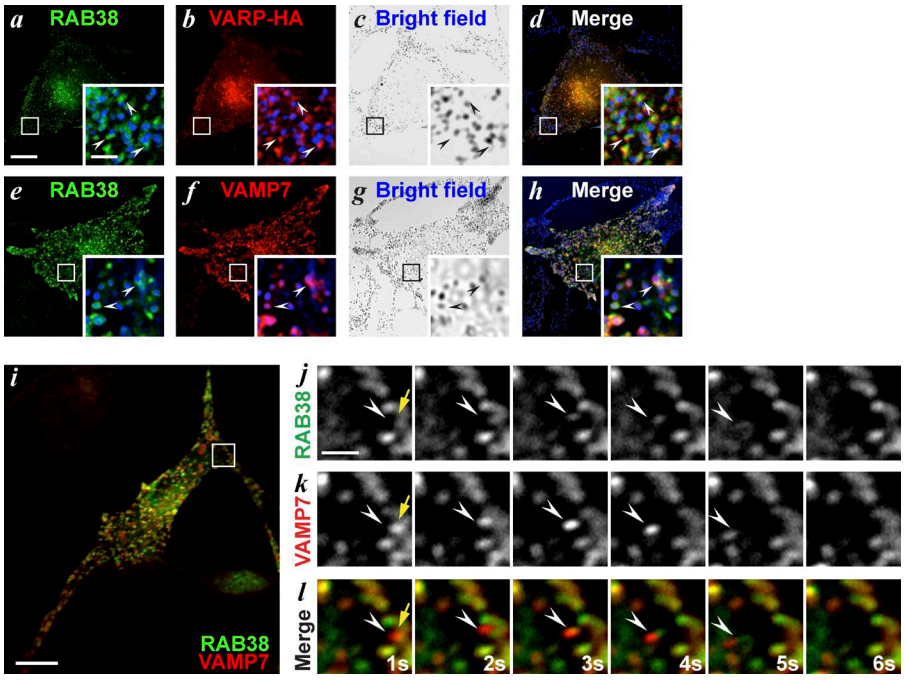

Figure 7. **RAB38 overlaps with VARP on melanosomes and accompanies GFP-VAMP7 on departing tubules.** (a–l) WT melan-Ink4a cells transiently transfected with GFP-RAB38 (green) and either VARP-HA (red, a–d), or mCh-VAMP7 (red, e–l) were analyzed 48 h later. (a–h) Cells were fixed, labeled with anti-HA (a–d), and analyzed by deconvolution immuno-FM. BF images are pseudocolored blue in merge and insets (boxed regions magnified five times). (a–d) Arrowheads show VARP-HA and GFP-RAB38 puncta adjacent to melanosomes. (e–h) Arrowheads show GFP-RAB38 and mCh-VAMP7 localized to melanosomes. (i–l) Cells were analyzed by spinning-disk confocal microscopy at ∼1 fps. (j–l) Image sequence of boxed region in i, magnified five times; elapsed time (in seconds) is indicated at the lower right. A mCh-VAMP7/GFP-RAB38–labeled structure (arrowhead) emerges from a mCh-VAMP7–labeled melanosome (arrow). Bars: (main) 10 µm; (insets and j–l) 2 µm.

Downloaded from on October 24, 2016

Published August 1, 2016

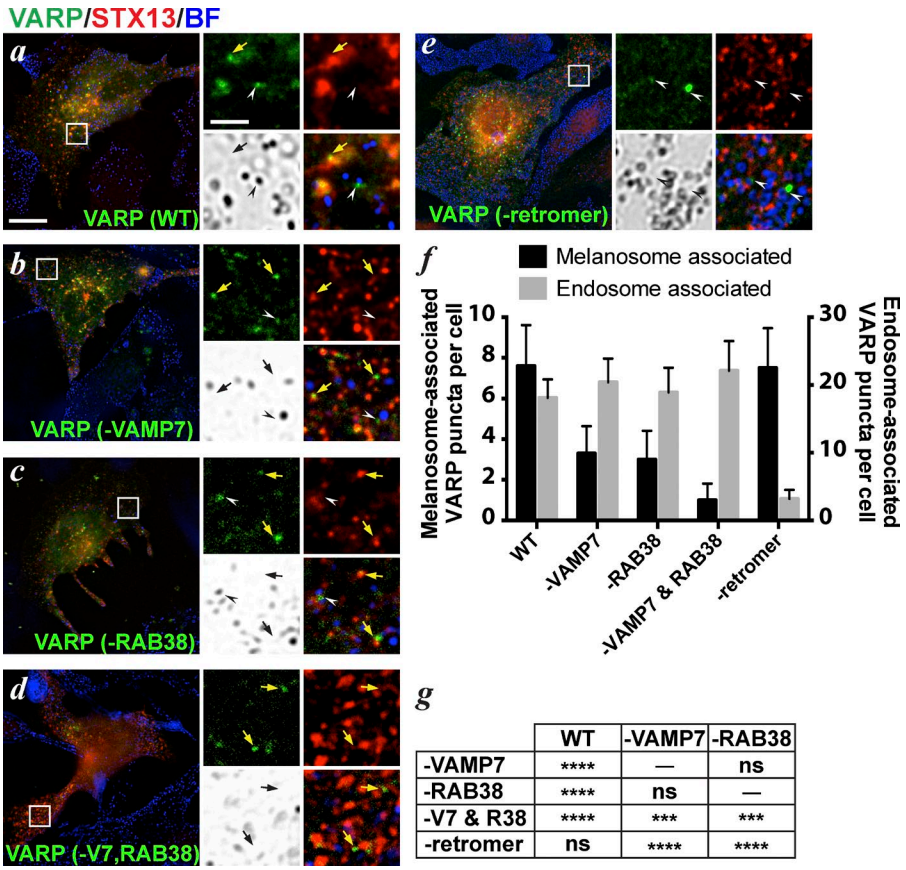

	WT	-VAMP7	-RAB38
-VAMP7	****	—	ns
-RAB38	****	ns	—
-V7 & R38	****	***	***
-retromer	ns	****	****

Figure 8. **VARP localizes to melanosomes by interaction with both VAMP7 and RAB38.** (a–g) WT melan-Ink4a cells were transiently transfected with mCh-STX13 (red) and either WT VARP-GFP (green, a) or site-directed mutants (green, b–e) with interfering mutations in the binding sites for VAMP7 (-VAMP7, b), RAB38 (-RAB38, c), both VAMP7 and RAB38 (-V7, RAB38, d), or the VPS29 retromer subunit (-retromer, e). Cells were fixed 48 h after transfection and analyzed by deconvolution FM; bar, 10 µm. Insets are boxed regions magnified five times. Bar, 2 µm. BF images are pseudocolored blue in merged images. Arrowheads show VARP-GFP puncta adjacent to melanosomes visualized by BF, and arrows point to VARP-GFP puncta adjacent to mCh-STX13-labeled endosomes. (f) WT or mutant VARP-GFP puncta that were associated with melanosomes (visualized by BF; black bars) or with endosomes (labeled by mCh-STX13; gray bars) were quantified as mean ± SD from 10 cells per VARP variant representing three independent experiments. (g) P-values for pairwise comparisons of melanosome-associated VARP puncta in f. For endosome-associated VARP, only -V7 & R38 ($P < 0.05$ vs. WT) and -retromer ($P < 0.0001$ vs. all others) showed significant differences.

2008). Here, we visualized the retrieval of VAMP7 from melanosomes in small tubular intermediates. Melanosomal cargoes were not enriched in these tubules, indicating that the tubules are cargo selective. VARP association with these tubules implies that VAMP7 within them is bound to VARP and thus inactive (Schäfer et al., 2012), as expected for a recycling v-SNARE. We speculate that VARP is released before fusion with the target, allowing VAMP7 to serve as a v-SNARE during recycling. We could not visualize the target compartment of these rapidly motile tubules by single-plane spinning-disc microscopy, but we speculate that they ultimately return VAMP7 to STX13-containing early endosomes either directly or via late endosomes or the plasma membrane. It is also unclear how cargo is selected for entry into the tubules but AP-3, which engages VAMP7 on early endosomes (Martinez-Arca et al., 2003; Kent et al., 2012) and was recently suggested to facilitate STX13 recycling from melanosomes (Jani et al., 2015), is unlikely to participate in this process, as VAMP7 is localized normally in AP-3–deficient melanocytes (unpublished data). VARP itself might sort VAMP7 into the tubules; testing this model will require reconstitution of VARP-deficient melanocytes with specific binding mutants.

The dramatic depletion of VAMP7-containing recycling tubules in cells lacking BLOC-3 suggests that RAB38 and/or RAB32 play an important role in recruiting effectors for cargo selection, tubule formation, and/or tubule release. One such effector might be the RAB32/38 binding partner myosin Vc (Bultema et al., 2014), which might primarily mediate recycling tubule dynamics with secondary effects on melanosome secretion (Bultema et al., 2014). RAB38 and VAMP7 might indirectly engage other recycling effectors via VARP, akin to the recruitment of the kinesin-1 motor KIF5 by VARP in neurons (Burgo et al., 2012). The ubiquitously expressed BLOC-3 (Chiang et al., 2003; Martina et al., 2003; Nazarian et al., 2003) might facilitate VAMP7 retrieval from other organelles in cell types that lack LROs, perhaps through activation of trace levels of RAB32 or RAB38 or of a distinct RAB. Note that although binding to retromer was not required for VARP recruitment to melanosomes, our data do not negate a role for retromer in either anterograde or retrograde transport as recently proposed (McGough et al., 2014).

Although BLOC-3 clearly functions as a GEF for RAB32 and RAB38 (Gerondopoulos et al., 2012), the physiological roles of BLOC-3 and its target RABs during melanosome biogenesis were unknown. Simultaneous depletion of RAB32 and RAB38 (Loftus et al., 2002; Wasmeier et al., 2006; Bultema et al., 2012) or VARP (Tamura et al., 2009, 2011) in skin melanocytes resulted in pigment dilution and TYR and TYRP1 mislocalization largely to the Golgi and/or TGN. Similarly, retinal pigment epithelia (RPE) from RAB38-deficient *chocolate* mice are depleted of melanosomes and mislocalize a cohort of TYR (Lopes et al., 2007), and MNT-1 melanoma cells depleted of RAB32, RAB38, or BLOC-3 subunits are severely hypopigmented (Gerondopoulos et al., 2012). These data were interpreted as a direct role for these proteins in anterograde traffic, but they could also be explained by an indirect role through a failure of VAMP7 recycling and its resulting entrapment on melanosomes; this would deplete VAMP7 from early endosomes with a consequent secondary failure in anterograde trafficking, as seen with VAMP7 knockdown (Tamura et al., 2011; Jani et al., 2015; Fig. 1). This model for a primary role for BLOC-3 and RAB38 in retrograde transport would be consistent with the localization of RAB32 and RAB38 primarily to melanosomes

Downloaded from on October 24, 2016

Published August 1, 2016

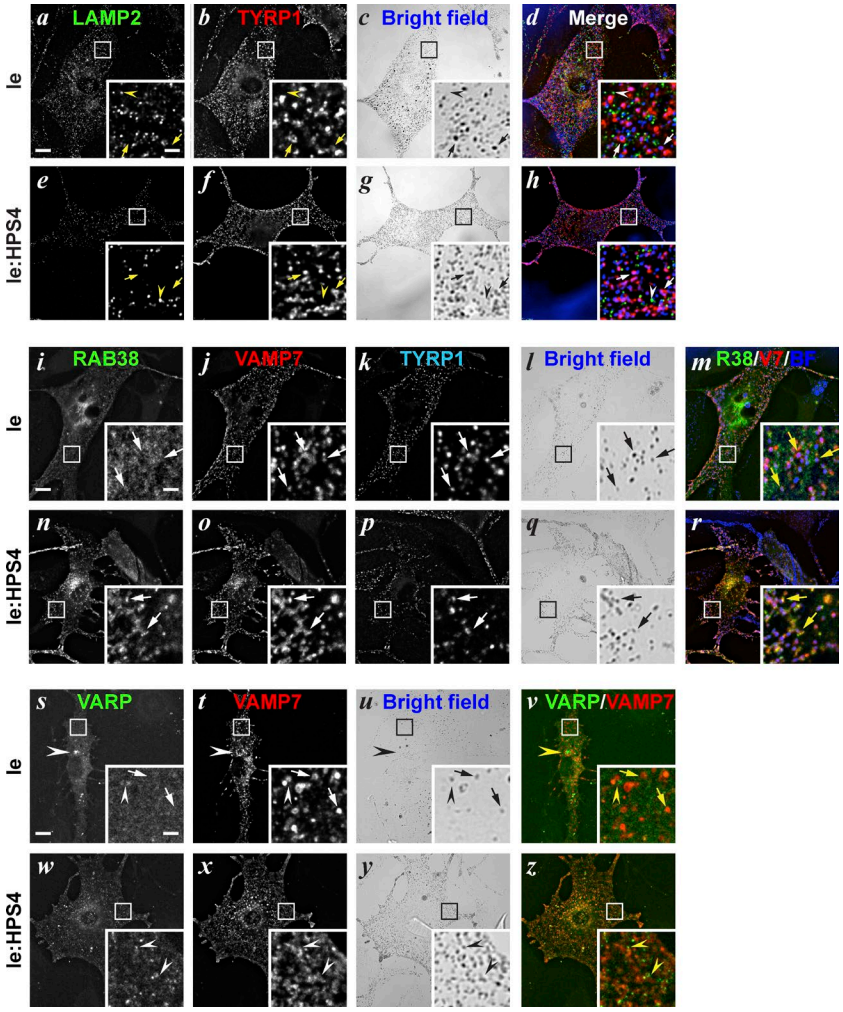

Figure 9. **VAMP7 and TYRP1, but not RAB38 and VARP, localize normally to melanosomes in BLOC-3–deficient cells.** (a–z) BLOC-3–deficient melan-le (le; a–d, i–m, and s–v) and "rescued" melan-le cells stably expressing HA-HPS4 (le:HPS4; e–h, n–r, and w–z) were untreated (a–h) or transiently transfected with mCh-VAMP7 (red, i–z) and either GFP-RAB38 (green, i–r) or VARP-GFP (green, s–z), fixed 24 h (a–r) or 48 h (s–z) after transfection, and immunolabeled for LAMP2 (green, a–h) and/or TYRP1 (red, a–h; cyan, i–r) and analyzed by deconvolution immuno-FM. (a–h) Arrowhead points to a LAMP2-positive lysosome, and arrows show TYRP1-positive melanosomes. (i–r) Arrows show mCh-VAMP7 and TYRP1 colocalized to melanosomes visualized by BF. Note RAB38-GFP localization to melanosomes in le:HPS4 (n), but not in le (i). (s–z) Large arrowhead in le main panel (s) shows perinuclear accumulation of VARP-GFP. Arrowheads in insets show VARP-GFP puncta associated with melanosomes, and arrows point to melanosomes lacking VARP-GFP puncta. BF images in c, g, l, and q are pseudocolored blue in the merged images in d, h, m, and r. Insets, boxed regions magnified five times. Bars: (main) 10 µm; (insets) 2 µm.

(Bultema et al., 2012; Gerondopoulos et al., 2012; Fig. 7, a–h) and secondarily to tubulovesicular membranes (Wasmeier et al., 2006) that might be retrograde, rather than anterograde, transport intermediates. The reported interactions of RAB38 and RAB32 with the anterograde trafficking factors AP-1, BLOC-1, and BLOC-2 (Bultema et al., 2012) might coordinate anterograde and retrograde trafficking.

Intriguingly, a primary role for BLOC-3 and RAB32/38 in VAMP7 recycling could also explain the variable phenotypes of pigment cells in BLOC-3–deficient mice (Gardner et al., 1997; Nguyen and Wei, 2007) and HPS patients (Anderson et al., 2003; Takeuchi et al., 2014). In eyes of BLOC-3–deficient *light ear* or *pale ear* mice, RPE harbor few small, lightly pigmented melanosomes, whereas melanocytes of the adjacent choroid contain highly pigmented macromelanosomes (Gardner et al., 1997; Suzuki et al., 2002). Similarly, *light ear* and *pale ear* hair bulb melanocytes (like the immortalized melan-ep and melan-le cells used here) harbor enlarged but otherwise normally pigmented melanosomes (Nguyen et al., 2002), whereas interfollicular skin melanocytes (like BLOC-3–depleted MNT-1 cells [Gerondopoulos et al., 2012] and HPS1 patient primary melanocytes [Boissy et al., 1998]) harbor fewer, small, hypopigmented melanosomes (Nguyen and Wei, 2007); these differences result in dark fur and light skin (Lane and Green, 1967). We speculate that these cell type–specific differences in melanosome biogenesis reflect different requirements for VAMP7 recycling in maintaining an endosomal pool of VAMP7 for anterograde transport. For example, cell types with low levels of VAMP7 expression and/or high rates of melanosome biogenesis would deplete VAMP7 from endosomes and hence block anterograde cargo trafficking required for melanosome maturation, resulting in fewer, smaller and hypopigmented melanosomes. Alternatively, cell types with high levels of VAMP7 expression and/or low rates of melanosome biogenesis might restore sufficient levels of endosomal VAMP7 biosynthetically to compensate for the loss of recycling and permit sufficient anterograde cargo delivery for melanosome synthesis. The enlarged melanosomes in such cells would result from (1) continued anterograde membrane delivery without compensating retrograde membrane retrieval and (2) fusion of melanosomes with each other and with other organelles because of an excess of "unprotected" fusogenic VAMP7 lacking VARP. A similar rationale might explain the differences in melanosome biogenesis in the RPE and choroidal melanocytes in RAB38-deficient *chocolate* mice (Brooks et al., 2007; Lopes et al., 2007) and, perhaps, the defect in TYRP1 localization in VARP-depleted melan-a cells (Tamura et al., 2009, 2011). Although future analyses of the rates of melanosome biogenesis and VAMP7 biosynthesis will be necessary to test these models, the identification of a VAMP7 recycling pathway from melanosomes that is regulated by BLOC-3 provides a new way of thinking about an old problem.

Downloaded from on October 24, 2016

Published August 1, 2016

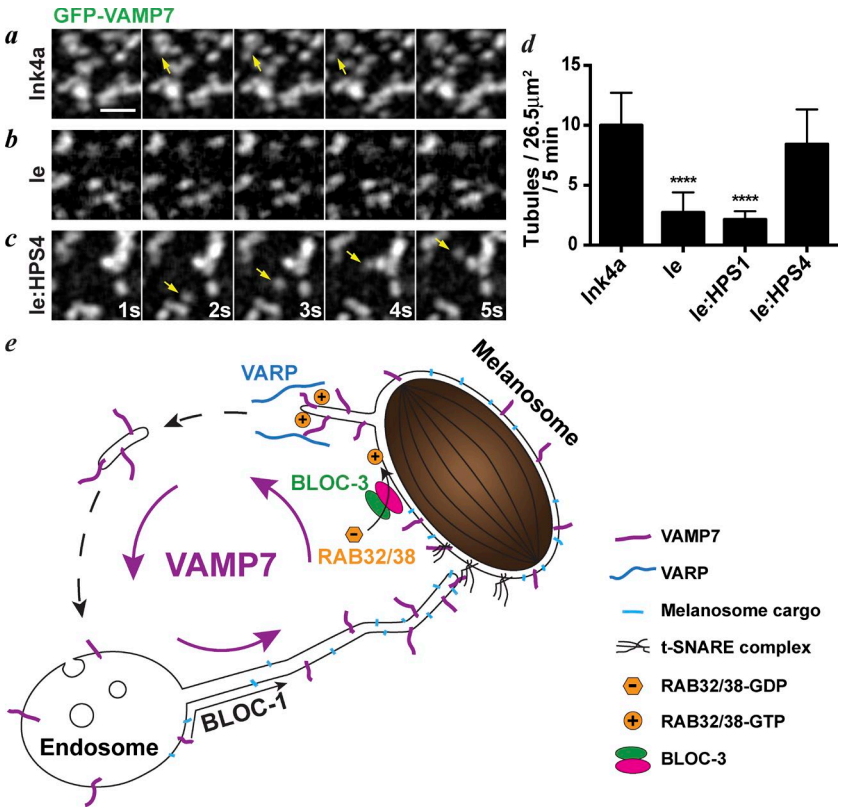

Figure 10. **BLOC-3 is required to retrieve VAMP7 from melanosomes.** (a–d) WT melan-Ink4a (Ink4a; a), melan-le (le; b), melan-le:HPS1 (le:HPS1; not depicted), or melan-le:HPS4 (le:HPS4; c) cells transiently transfected with GFP-VAMP7 were analyzed by spinning-disk confocal microscopy 24 h later. Images were acquired at ∼1 fps and a segment of the image sequence is shown. Elapsed time (in seconds) is indicated at lower right. Bar, 2 µm. Arrows show GFP-VAMP7–labeled structures exiting GFP-VAMP7–labeled melanosomes. (d) Fission of GFP-VAMP7 transport intermediates from melanosomes was quantified by counting events within 26.5-µm² regions in the cell periphery during 5-min image sequences acquired at 1 fps. At least 15 regions from a minimum of six cells, representing three independent experiments, were quantified for each cell type; shown are mean values ± SD. ****, P < 0.0001. (e) Model for VAMP7 cycling during melanosome biogenesis.

Materials and methods

Reagents

Chemicals were obtained from Sigma-Aldrich, except where noted. Hygromycin B was obtained from Roche. Tissue culture reagents and Lipofectamine 2000 were obtained from Invitrogen. Matrigel was obtained from BD.

Cell culture and generation of stable cells

Immortalized melanocyte cell lines melan-Ink4a-1 (also known as melan-Ink-4a-Arf-1; referred to here as melan-Ink4a or WT) derived from C57BL/6 *Ink4a-Arf*$^{-/-}$ mice (Sviderskaya et al., 2002), melan-ep1 (referred to here as melan-ep) derived from BLOC-3–deficient C57BL/6J *Hps1*$^{ep/ep}$ *pale ear* mice and melan-le1 (referred to here as melan-le) derived from BLOC-3–deficient C57BL/6J *Hps4*$^{le/le}$ *light ear* mice (Suzuki et al., 2002; Chiang et al., 2003), and melan-pa1 (referred to here as melan-pa) derived from BLOC-1–deficient C57BL/6J-*Pldn*$^{pa/pa}$ *pallid* mice, melan-mu1 (referred to here as melan-mu) derived from BLOC-1–deficient B6.CHMU/Le *Muted*$^{mu/mu}$ *muted* mice, and stably transduced melan-pa:myc-Pa and melan-mu:MuHA lines in which BLOC-1 function is restored via expression of the missing subunit (Setty et al., 2007) have been previously described. All cells were cultured in RPMI 1640 medium supplemented with 10% FBS (Atlanta Biologicals) and 200 nM 12-*O*-tetradecanoylphorbol-13-acetate. Melan-le, melan-ep, and stable lines derived from these cells were also cultured in the presence of 200 pM cholera toxin. Stably transduced cell lines were generated by infection with recombinant retroviruses produced in transiently transfected Plat-E cells (Morita et al., 2000) and selection with 100 µg/ml (for melan-ep based lines) or 150 µg/ml (for melan-le based lines) hygromycin B as described previously (Setty et al., 2007; Meng et al., 2012). Stable cell lines were occasionally treated with hygromycin B (100 or 150 µg/ml) to maintain selection for transgene expression. In most experiments, cells were transiently transfected with expression plasmids using Lipofectamine 2000 (1 µl with 800 ng DNA, including carrier DNA as needed, in 100 µl Opti-MEM for each coverslip in a 24-well plate or 4 µl Lipofectamine 2000 with 4 µg DNA in 500 µl Opti-MEM for 35-mm glass-bottom dishes) and imaged at varying times after transfection as indicated. Only cells with low or modest levels of transgene expression were chosen for analysis, and DNA amounts were titrated to ensure modest but detectable expression in 10–40% of transfected cells.

Antibodies

The following monoclonal antibodies were used: mouse anti-TYRP1 (TA99) from ATCC; rat anti-LAMP1 (1D4B) and rat anti-LAMP2 (GL2A7) from Developmental Studies Hybridoma Bank; mouse anti-PMEL (HMB-45) from Lab Vision; and mouse anti-HA.11 from Covance. Anti-VAMP7 mAb (158.2) and pAb (TG50) have previously been described and validated using *Vamp7*$^{-/-}$ mice (Danglot et al., 2012). Polyclonal rabbit antisera to STX13 (Prekeris et al., 1998) have been previously described, and rabbit anti-Giantin was purchased from Abcam (ab24586). Species-specific secondary antibodies from donkey conjugated to Alexa Fluor 488, 594, or 647 or Dylite 488, 594, or 647 used in immuno-FM were obtained from Jackson ImmunoResearch Laboratories, Inc.

DNA constructs and siRNAs

The siRNAs used were human VAMP7 siRNA (5′-CTGCCAAGA CAGGATTGTATA-3′; Danglot et al., 2010) and control siRNA (5′-AATTCTCCGAACGTGTCACGT-3′). Recombinant retroviral vectors pBMN-X/N-IRES-Hygro-HA3-hHPS1 and pBMN-X/N-IRES-Hygro-HA3-hHPS4 encoding human HPS1 and HPS4 under the control of the Maloney mouse leukemia virus promoter were generated by subcloning the XhoI–NotI cDNA fragment from pCI-HA3-humanHPS1 and pCI-HA3-humanHPS4 (gifts from J. Bonifacino, National Institutes of Health, Bethesda, MD) into pBMN-X/N-IRES-Hygro.

Downloaded from on October 24, 2016

Published August 1, 2016

pCR3-mRFP-OCA2, pmCh-C1-STX13, pEGFP-C1-STX13, and pEGFP-N1-TYRP-EGFP (Dennis et al., 2015); pBMN-IRES-Hygro-mycPa and pBMN-IRES-Hygro-mycMu (Setty et al., 2007); pLXIN-huVARP-HA2 (Schäfer et al., 2012); and pLXIN-huVARP-EGFP, pLXIN-huVARP(M684D,Y687S)-EGFP, pLXIN, huVARP(Q509A, Y550A)-EGFP, pLXIN-huVARP(H432S,L434A,H712S,L714A)-EGFP, and pEGFP-N1-VARP(WT)-EGFP (Hesketh et al., 2014) have been previously described. pmRFP-N1-TYRP-mRFP was generated by amplifying mRFP from pmRFP-N1 by PCR and subcloning the resulting SalI–NotI fragment into pEGFP-N1-huTYRP1. pEGFP-C2-RAB38 was a gift from A. Hume (University of Nottingham, Nottingham, England, UK). mCh-RAB38 controlled by the cytomegalovirus immediate early (CMV) promoter was generated by subcloning mCh into pEGFP-C2-RAB38 using the AgeI–XhoI region of mCh from pmCh-C1 (Takara Bio Inc.). pLXIN-VAMP4-HA (Gordon et al., 2009) was a gift from A. Peden (University of Sheffield, Sheffield, England, UK). EGFP-VAMP2, EGFP-VAMP7, and EGFP-VAMP8 in pEGFP-C vector, controlled by the CMV promoter and generated from rat cDNA, were gifts from P. Roche (National Institutes of Health, Bethesda, MD). pmCh-VAMP7 controlled by the CMV promoter was generated by subcloning mCh into pEGFP-C-VAMP7 using the AgeI–BsrGI region of mCh from pmCh-C1 (Takara Bio Inc.).

EM

For conventional EM, MNT-1 cells were fixed with 2.5% glutaraldehyde in 0.1 M cacodylate buffer (1.5 h on ice), postfixed with 1% OsO_4/1.5% potassium ferricyanide (45 min on ice), dehydrated in ethanol, and embedded in epon resin. For ultrathin cryosectioning, MNT-1 cells fixed with 2% PFA and 0.2% glutaraldehyde in 0.1 M phosphate buffer (pH 7.4) were processed for ultracryomicrotomy and immunogold labeled using TYRP1 antibody (TA99) followed by protein A conjugated to 10 nm gold (PAG10). Electron micrographs were acquired using Philips CM120 or Tecnai Spirit G2 (FEI) equipped with a numeric camera (Keen View; Soft Imaging System) or 4k charge coupled device camera (Quemesa; Olympus).

Immunoblotting

MNT-1 cells were seeded at 10^6 per 10-cm Petri dish and transfected with Oligofectamine (Invitrogen) 2 d later with control- or VAMP7-specific siRNAs and then again after an additional 3 d. 3 d later, cells were washed in cold PBS and incubated in cold lysis buffer (50 mM Tris, 150 mM NaCl, 0.1% Triton X-100, and 10 mM EDTA, pH 7.2, supplemented with protease inhibitor cocktail [Roche]) for 20 min on ice. Cell lysates were collected by scraping and clarified by centrifugation for 15 min at 13,000 rpm (4°C). Lysates were incubated with sample buffer (2× concentrated), boiled for 5 min, and processed for immunoblotting.

Quantification of melanin content

MNT-1 cells were seeded at 10^5 per well in a six-well plate and transfected twice with siRNA as for immunoblotting. 3 d after the second siRNA transfection, cells were washed twice in cold PBS and incubated with 200 µl cold melanin buffer (50 mM Tris, 150 mM NaCl, and 2 mM EDTA, pH 7.2). Cells were scraped and sonicated, and 100 µl lysate was centrifuged at 13,000 rpm for 15 min at 4°C. Supernatants were removed and pellets washed with 500 µl ethanol/ether (1:1 ratio) and dissolved in 230 µl 2 M NaOH/20% DMSO for 1 h at 60°C. The optical density at 490 nm of 200 µl of solubilized melanin was measured and normalized to protein content evaluated by Bradford assay (Thermo Fisher Scientific).

FM

Standard immuno-FM and colocalization analyses. Cells were plated on Matrigel-coated coverslips, fixed with 3% PFA in Hank's buffered salt solution, labeled with primary and secondary antibodies and mounted using Vectashield H-1000 (Vector Laboratories). Cells were analyzed by epifluorescence microscopy on a DM IRBE or DMI 6000B microscope (Leica Biosystems) equipped with a 63× Plan Apochromat objective (1.4 NA) and either a Retiga EXi Fast 1394 or a Hamamatsu Photonics ORCA-Flash4.0 sCMOS digital camera. Images were acquired in z-stacks using a 0.2-µm (DM IRBE) or 0.19-µm (DMI 6000B) step size and deconvolved using either subtractive volume deconvolution with OpenLab (PerkinElmer) software or Gold's Method deconvolution with three iterations in LASX (Leica Biosystems) software.

Quantification of overlap between markers in melanosomes. Quantification of the area of overlap in the cell periphery between two fluorescent labels or a fluorescent label and pigmented melanosomes was performed using ImageJ (National Institutes of Health) on widefield fluorescence images using a method similar to that previously used with OpenLab software (Setty et al., 2007). In brief, images were cropped to contain a single cell with the nucleus and perinuclear area removed, and binary images of fluorescence were generated by subtracting the local background before thresholding using parameters of a rolling ball radius of 10 pixels with smoothing disabled. Binary images of pigment granules from BF imaging were generated by manual thresholding. The Image Calculator function was used to generate an image representing the area of overlap between channels by multiplying the binary images for each of the two channels. The areas of overlap and of total fluorescent labeling in structures larger than five pixels were quantified using the Analyze Particles function; the ratio of overlap pixels to total fluorescent pixels in the channel of interest gives the percentage of overlap.

Transient rescue of BLOC-1$^-$ cells expressing GFP-VAMP7, TYRP-GFP, and mCh-STX13. BLOC-$1^{-/-}$ melan-pa cells were seeded on Matrigel-coated coverslips in 24-well tissue culture plates and 24 h later transiently transfected with Lipofectamine using 200 ng each of pEGFP-C-VAMP7 and pmCh-C1-STX13 and 500 ng of either pBMN-IRES-Hygro-mycMu or pBMN-IRES-Hygro-mycPa. At indicated times after transfection, cells were fixed with 3% PFA in Hank's buffered salt solution and either mounted directly using Vectashield or processed for standard immuno-FM as described above with either TA99 or HMB-45 and Dylite647-conjugated secondary antibodies. Cells were imaged as for standard immuno-FM. The number of GFP-VAMP7-positive, mCH-STX13-negative puncta was quantified by manual counting within selected 200 × 200–pixel regions in the periphery of cells. Quantification of overlap between GFP-VAMP7 and mCh-STX13 in the cell periphery was completed as described above for Standard immuno-FM and colocalization analyses.

Quantification of melanosomal and endosomal VARP localization using site-directed VARP mutants. WT melan-Ink4a melanocytes were seeded on Matrigel-coated coverslips and transfected using Lipofectamine 2000 with mCh-STX13 and either pLXIN-VARP(WT)-EGFP or the site-directed pLXIN-VARP-GFP mutants deficient for binding to VAMP7 only, RAB38 only, both VAMP7 and RAB38, or retromer. 48 h after transfection, cells were fixed and processed for standard immuno-FM and deconvolved using LASX and Gold's method (three iterations). Quantification of VARP-GFP puncta associated with melanosomes visualized by BF microscopy or associated with mCh-STX13–labeled endosomes was done by manual counting after excluding a 200-pixel-diameter circular selection containing the nucleus and Golgi region.

Live-cell imaging

Cells were seeded in Matrigel-coated 35-mm glass-bottom dishes and transiently transfected with indicated GFP- or mCh/mRFP-fusion proteins using Lipofectamine 2000. At indicated times after transfection,

Downloaded from on October 24, 2016

Published August 1, 2016

cells in riboflavin-free RPMI (US Biological) containing 10% FBS were imaged on a Axiovert 200 microscope (ZEISS) equipped with a 63X Plan-Apo objective lens (NA 1.4), an UltraVIEW ERS6 spinning-disk confocal scan head (PerkinElmer), an environmental chamber at 37°C, an Orca ER CCD camera (Hamamatsu Photonics) and Volocity (PerkinElmer) software for image acquisition. In some experiments, an ORCA-Flash4.0 sCMOS camera was used instead. For imaging of cells expressing GFP-VAMP7 relative to melanosomes imaged by BF microscopy (Fig. 5, a–c; and Fig. S2 i), we used an Olympus IX71 spinning-disk confocal microscope equipped with a 100× Plan-Apo objective (NA 1.4), LCI Chamlide stagetop incubation chamber at 37°C/5% CO_2, an ImageEM EM-CCD camera (Hamamatsu Photonics), and MetaMorph (Molecular Devices) software for image acquisition. Image sequences were further analyzed using ImageJ. All images were captured at ∼1 frames per second (fps) except for Video 9, which was captured at ∼1.4 fps.

Quantification of GFP-VAMP7 and mCh-STX13 tubule length and stability

To quantify the length and stability of GFP-VAMP7 and mCh-STX13 tubules in WT melan-Ink4a melanocytes, cells were seeded in Matrigel-coated 35 mm glass-bottom dishes, cotransfected with GFP-VAMP7 and mCh-STX13 and imaged 24 h later as described in the section above at ∼1 fps. Tubule length was measured by tracing the tubule at its maximum length using the "Measure" command in ImageJ, and tubule stability was measured by counting the total number of frames in which an identifiable tubule was present. 50 total tubules (five tubules from each of ten cells, acquired on at least three independent days) were quantified for each type of tubule.

Quantification of GFP-VAMP7 tubules leaving melanosomes

To quantify the number of GFP-VAMP7 tubules leaving melanosomes in WT, BLOC-3–deficient, and BLOC-3–rescued cells, cells were seeded on Matrigel-coated 35-mm glass-bottom plates, transfected with GFP-VAMP7 using Lipofectamine 2000, and imaged 24 h after transfection. Image sequences were acquired for 5 min at ∼1 fps (300 images) as described above in the Live-cell imaging section. Quantification was completed using ImageJ Fiji. First, the perinuclear region of each cell was excluded by placing a circular region of interest with diameter 200 pixels over the nucleus and adjacent Golgi region as visualized by an accumulation of GFP-VAMP7 signal. 50 × 50–pixel regions were selected and cropped from the periphery of each cell, avoiding the nuclear ROI and edges of the cell. Local background was subtracted from these 50-pixel-square regions using the "Process -> Subtract Background" command in ImageJ with settings of rolling ball radius of 10 pixels, and a sliding parabola with all other boxes unchecked; the resulting "background subtracted" file was further processed using the "Smooth" command to yield a "smoothed" file. The "Combine" command was then used to place the "background subtracted" and "smoothed" files adjacent to each other, and only fission of tubules that were observed in both files were included in the quantification. For quantification, the number of GFP-VAMP7 tubules/vesicles observed to depart from GFP-VAMP7–labeled melanosomes was manually counted over all 300 frames of an image sequence.

Statistical analysis

Statistical significance was determined by the unpaired two-tailed Student's *t* test. All values are indicated as ± SD. *, $P < 0.05$; **, $P < 0.01$; ***, $P < 0.005$; and ****, $P < 0.0001$.

Online supplemental material

Fig. S1 provides supporting evidence that VAMP7 resides in melanosomes and that it is trapped in early endosomes in a second BLOC-1–deficient model. Fig. S2 shows a still image of the entire cell from a frame of an image sequence of GFP-VAMP7 or TYRP1-GFP and mCh-STX13 in WT cells, an inset of which is shown in Fig. 4 and Videos 1 and 2; a corresponding image sequence of GFP-VAMP7 and mCh-STX13 in BLOC-1–deficient cells as a control, also seen in Video 5; quantification of GFP-VAMP7 and mCh-STX13 tubule length and stability in WT melan-Ink4a melanocytes; still images of the entire cell from the first frame of image sequences of insets shown in Fig. 5, and Videos 6 and 7; and an image sequence in which a GFP-VAMP7–labeled tubule emerges from a melanosome labeled by mRFP-OCA2, supporting Fig. 5 and Video 8. Fig. S3 shows the entire cell from the first frame of image sequences, insets of which are shown in Fig. 6 and Videos 9 and 11, and shows image sequences derived from Video 10, in which a tubule marked by VARP-GFP, but not TYRP1-mRFP, exits a melanosome. Fig. S4 shows representative localization of the lysosomal protein LAMP2 and the melanosomal protein TYRP1 in WT and BLOC-3–deficient le:HPS1 and images from HPS4-deficient le melanocytes mock-rescued by expression of the BLOC-3 subunit HPS1 (le:HPS1) in which neither RAB38-GFP nor VARP-GFP localization is restored to melanosomes, supporting Fig. 9. Fig. S5 provides supporting evidence that VARP and RAB38, but not VAMP7, are mislocalized and depleted from melanosomes in a second BLOC-3-deficient cell model. Video 1 shows that GFP-VAMP7 and mCh-STX13 label separate tubule populations in WT melanocytes. Video 2 shows that TYRP1-GFP is undetectable in anterograde mCh-STX13 tubules in WT melanocytes. Video 3 shows that GFP-VAMP7 is detected in mCh-STX13 tubules in transiently rescued melan-pa melanocytes with restored BLOC-1 function. Video 4 shows that TYRP1-GFP is detected in mCh-STX13 tubules in transiently rescued melan-pa melanocytes with restored BLOC-1 function. Video 5 shows that GFP-VAMP7 and mCh-STX13 are retained in enlarged endosomes and that mCh-STX13 tubules are dramatically reduced in in BLOC-1–deficient melanocytes. Video 6 shows that GFP-VAMP7–labeled tubules exit pigmented melanosomes. Video 7 shows that TYRP1-mRFP is undetectable in GFP-VAMP7–labeled tubules that emerge from melanosomes labeled by GFP-VAMP7 and TYRP1-mRFP. Video 8 shows that mRFP-OCA2 is undetectable in GFP-VAMP7-labeled tubules that emerge from melanosomes labeled by GFP-VAMP7 and mRFP-OCA2. Video 9 shows that mCh-VAMP7 tubules are also labeled by VARP-GFP. Video 10 shows that TYRP1-mRFP is undetectable in VARP-GFP–labeled tubules that emerge from TYRP1-mRFP–labeled melanosomes. Video 11 shows that mRFP-OCA2 is undetectable in VARP-GFP–labeled tubules that emerge from mRFP-OCA2–labeled melanosomes. Video 12 shows that VARP-GFP labels tubules that originate from STX13-labeled endosomes but that these tubules are distinct from those that are labeled by mCh-STX13 and destined for melanosomes. Video 13 shows that GFP-RAB38 is present on mCh-VAMP7–containing tubules that emerge from melanosomes. Video 14 shows examples of regions of interest for quantification of GFP-VAMP7 tubules departing melanosomes in WT, le:HPS1, and le:HPS4 melanocytes for analyses shown in Fig. 10 d. Online supplemental material is available at http://www.jcb.org/cgi/content/full/jcb.201605090/DC1.

Downloaded from on October 24, 2016

Acknowledgments

We thank A. Stout (Penn Cell and Developmental Biology Microscopy Core) and J. Burkhardt for use of spinning-disc microscopes; the Nikon Imaging Center at Institut Curie-Centre National de la Recherche Scientifique and The BioImaging Cell and Tissue Core Facility (PICT-IBiSA), supported by the CelTisPhyBio Labex (ANR-10-LBX-0038) and IDEX Paris Sciences et Lettres Research University (ANR-10-IDEX-0001-02); J. Bonifacino, A. Hume, A. Peden, and P. Roche for gifts of reagents; and A. Mantegazza and D. Harper for technical help.

Published August 1, 2016

This work was supported by grants from the National Institutes of Health, National Eye Institute (R01 EY015625, to M.S. Marks and G. Raposo), National Institute of Arthritis and Musculoskeletal and Skin Diseases (R01 AR048155, to M.S. Marks, and F32 AR062476, to M.K. Dennis), National Institute of General Medical Sciences (R01 GM108807, to M.S. Marks); Fondation pour la Recherche Médicale (to T. Galli); the UK Medical Research Council (G0900113, to J.P. Luzio); and the Wellcome Trust (108429, to E.V. Sviderskaya and D.C. Bennett). This work was also supported by a Canadian Institutes of Health Research Fellowship (to G.G. Hesketh) and a Fondation pour la Recherche Médicale grant from Centre National de la Recherche Scientifique, Institut National de la Santé et de la Recherche Médicale, Institut Curie, and Fondation pour la Recherche Médicale (DEQ20140329491 Team label, to G. Raposo).

The authors declare no competing financial interests.

Submitted: 23 May 2016
Accepted: 11 July 2016

References

Anderson, P.D., M. Huizing, D.A. Claassen, J. White, and W.A. Gahl. 2003. Hermansky-Pudlak syndrome type 4 (HPS-4): clinical and molecular characteristics. *Hum. Genet.* 113:10–17.

Barlowe, C.K., and E.A. Miller. 2013. Secretory protein biogenesis and traffic in the early secretory pathway. *Genetics.* 193:383–410. http://dx.doi.org/10.1534/genetics.112.142810

Bennett, D.C., P.J. Cooper, and I.R. Hart. 1987. A line of non-tumorigenic mouse melanocytes, syngeneic with the B16 melanoma and requiring a tumour promoter for growth. *Int. J. Cancer.* 39:414–418. http://dx.doi.org/10.1002/ijc.2910390324

Boissy, R.E., Y. Zhao, and W.A. Gahl. 1998. Altered protein localization in melanocytes from Hermansky-Pudlak syndrome: support for the role of the HPS gene product in intracellular trafficking. *Lab. Invest.* 78:1037–1048.

Bonifacino, J.S., and B.S. Glick. 2004. The mechanisms of vesicle budding and fusion. *Cell.* 116:153–166. http://dx.doi.org/10.1016/S0092-8674(03)01079-1

Bright, N.A., M.J. Gratian, and J.P. Luzio. 2005. Endocytic delivery to lysosomes mediated by concurrent fusion and kissing events in living cells. *Curr. Biol.* 15:360–365. http://dx.doi.org/10.1016/j.cub.2005.01.049

Brooks, B.P., D.M. Larson, C.C. Chan, S. Kjellstrom, R.S. Smith, M.A. Crawford, L. Lamoreux, M. Huizing, R. Hess, X. Jiao, et al. 2007. Analysis of ocular hypopigmentation in Rab38cht/cht mice. *Invest. Ophthalmol. Vis. Sci.* 48:3905–3913. http://dx.doi.org/10.1167/iovs.06-1464

Bultema, J.J., A.L. Ambrosio, C.L. Burek, and S.M. Di Pietro. 2012. BLOC-2, AP-3, and AP-1 function in concert with Rab38 and Rab32 to mediate protein trafficking to lysosome-related organelles. *J. Biol. Chem.* 287:19550–19563. http://dx.doi.org/10.1074/jbc.M112.351908

Bultema, J.J., J.A. Boyle, P.B. Malenke, F.E. Martin, E.C. Dell'Angelica, R.E. Cheney, and S.M. Di Pietro. 2014. Myosin vc interacts with Rab32 and Rab38 proteins and works in the biogenesis and secretion of melanosomes. *J. Biol. Chem.* 289:33513–33528. http://dx.doi.org/10.1074/jbc.M114.578948

Burgo, A., E. Sotirakis, M.C. Simmler, A. Verraes, C. Chamot, J.C. Simpson, L. Lanzetti, V. Proux-Gillardeaux, and T. Galli. 2009. Role of Varp, a Rab21 exchange factor and TI-VAMP/VAMP7 partner, in neurite growth. *EMBO Rep.* 10:1117–1124. http://dx.doi.org/10.1038/embor.2009.186

Burgo, A., V. Proux-Gillardeaux, E. Sotirakis, P. Bun, A. Casano, A. Verraes, R.K. Liem, E. Formstecher, M. Coppey-Moisan, and T. Galli. 2012. A molecular network for the transport of the TI-VAMP/VAMP7 vesicles from cell center to periphery. *Dev. Cell.* 23:166–180. http://dx.doi.org/10.1016/j.devcel.2012.04.019

Cai, H., K. Reinisch, and S. Ferro-Novick. 2007. Coats, tethers, Rabs, and SNAREs work together to mediate the intracellular destination of a transport vesicle. *Dev. Cell.* 12:671–682. http://dx.doi.org/10.1016/j.devcel.2007.04.005

Chen, Y.A., and R.H. Scheller. 2001. SNARE-mediated membrane fusion. *Nat. Rev. Mol. Cell Biol.* 2:98–106. http://dx.doi.org/10.1038/35052017

Chiang, P.-W., N. Oiso, R. Gautam, T. Suzuki, R.T. Swank, and R.A. Spritz. 2003. The Hermansky-Pudlak syndrome 1 (HPS1) and HPS4 proteins are components of two complexes, BLOC-3 and BLOC-4, involved in the biogenesis of lysosome-related organelles. *J. Biol. Chem.* 278:20332–20337. http://dx.doi.org/10.1074/jbc.M300090200

Cullinane, A.R., J.A. Curry, C. Carmona-Rivera, C.G. Summers, C. Ciccone, N.D. Cardillo, H. Dorward, R.A. Hess, J.G. White, D. Adams, et al. 2011. A BLOC-1 mutation screen reveals that PLDN is mutated in Hermansky-Pudlak Syndrome type 9. *Am. J. Hum. Genet.* 88:778–787. http://dx.doi.org/10.1016/j.ajhg.2011.05.009

Danglot, L., M. Chaineau, M. Dahan, M.C. Gendron, N. Boggetto, F. Perez, and T. Galli. 2010. Role of TI-VAMP and CD82 in EGFR cell-surface dynamics and signaling. *J. Cell Sci.* 123:723–735. http://dx.doi.org/10.1242/jcs.062497

Danglot, L., K. Zylbersztejn, M. Petkovic, M. Gauberti, H. Meziane, R. Combe, M.F. Champy, M.C. Birling, G. Pavlovic, J.C. Bizot, et al. 2012. Absence of TI-VAMP/Vamp7 leads to increased anxiety in mice. *J. Neurosci.* 32:1962–1968. http://dx.doi.org/10.1523/JNEUROSCI.4436-11.2012

Delevoye, C., I. Hurbain, D. Tenza, J.-B. Sibarita, S. Uzan-Gafsou, H. Ohno, W.J.C. Geerts, A.J. Verkleij, J. Salamero, M.S. Marks, and G. Raposo. 2009. AP-1 and KIF13A coordinate endosomal sorting and positioning during melanosome biogenesis. *J. Cell Biol.* 187:247–264. http://dx.doi.org/10.1083/jcb.200907122

Delevoye, C., X. Heiligenstein, L. Ripoll, F. Gilles-Marsens, M.K. Dennis, R.A. Linares, L. Derman, A. Gokhale, E. Morel, V. Faundez, et al. 2016. BLOC-1 brings together the actin and microtubule cytoskeletons to generate recycling endosomes. *Curr. Biol.* 26:1–13. http://dx.doi.org/10.1016/j.cub.2015.11.020

Dell'Angelica, E.C. 2004. The building BLOC(k)s of lysosomes and related organelles. *Curr. Opin. Cell Biol.* 16:458–464. http://dx.doi.org/10.1016/j.ceb.2004.05.001

Dennis, M.K., A.R. Mantegazza, O.L. Snir, D. Tenza, A. Acosta-Ruiz, C. Delevoye, R. Zorger, A. Sitaram, W. de Jesus-Rojas, K. Ravichandran, et al. 2015. BLOC-2 targets recycling endosomal tubules to melanosomes for cargo delivery. *J. Cell Biol.* 209:563–577. http://dx.doi.org/10.1083/jcb.201410026

Di Pietro, S.M., and E.C. Dell'Angelica. 2005. The cell biology of Hermansky-Pudlak syndrome: recent advances. *Traffic.* 6:525–533. http://dx.doi.org/10.1111/j.1600-0854.2005.00299.x

Domanska, M.K., V. Kiessling, and L.K. Tamm. 2010. Docking and fast fusion of synaptobrevin vesicles depends on the lipid compositions of the vesicle and the acceptor SNARE complex-containing target membrane. *Biophys. J.* 99:2936–2946. http://dx.doi.org/10.1016/j.bpj.2010.09.011

Fader, C.M., D.G. Sánchez, M.B. Mestre, and M.I. Colombo. 2009. TI-VAMP/VAMP7 and VAMP3/cellubrevin: two v-SNARE proteins involved in specific steps of the autophagy/multivesicular body pathways. *Biochim. Biophys. Acta.* 1793:1901–1916. http://dx.doi.org/10.1016/j.bbamcr.2009.09.011

Fader, C.M., M.O. Aguilera, and M.I. Colombo. 2012. ATP is released from autophagic vesicles to the extracellular space in a VAMP7-dependent manner. *Autophagy.* 8:1741–1756. http://dx.doi.org/10.4161/auto.21858

Gardner, J.M., S.C. Wildenberg, N.M. Keiper, E.K. Novak, M.E. Rusiniak, R.T. Swank, N. Puri, J.N. Finger, N. Hagiwara, A.L. Lehman, et al. 1997. The mouse pale ear (ep) mutation is the homologue of human Hermansky-Pudlak syndrome. *Proc. Natl. Acad. Sci. USA.* 94:9238–9243. http://dx.doi.org/10.1073/pnas.94.17.9238

Gerondopoulos, A., L. Langemeyer, J.-R. Liang, A. Linford, and F.A. Barr. 2012. BLOC-3 mutated in Hermansky-Pudlak syndrome is a Rab32/38 guanine nucleotide exchange factor. *Curr. Biol.* 22:2135–2139. http://dx.doi.org/10.1016/j.cub.2012.09.020

Ghiani, C.A., M. Starcevic, I.A. Rodriguez-Fernandez, R. Nazarian, V.T. Cheli, L.N. Chan, J.S. Malvar, J. de Vellis, C. Sabatti, and E.C. Dell'Angelica. 2010. The dysbindin-containing complex (BLOC-1) in brain: developmental regulation, interaction with SNARE proteins and role in neurite outgrowth. *Mol. Psychiatry.* 15:115: 204–215. http://dx.doi.org/10.1038/mp.2009.152

Gordon, D.E., M. Mirza, D.A. Sahlender, J. Jakovleska, and A.A. Peden. 2009. Coiled-coil interactions are required for post-Golgi R-SNARE trafficking. *EMBO Rep.* 10:851–856. http://dx.doi.org/10.1038/embor.2009.96

Hesketh, G.G., I. Pérez-Dorado, L.P. Jackson, L. Wartosch, I.B. Schäfer, S.R. Gray, A.J. McCoy, O.B. Zeldin, E.F. Garman, M.E. Harbour, et al. 2014. VARP is recruited on to endosomes by direct interaction with retromer, where together they function in export to the cell surface. *Dev. Cell.* 29:591–606. http://dx.doi.org/10.1016/j.devcel.2014.04.010

Huang, L., Y.M. Kuo, and J. Gitschier. 1999. The pallid gene encodes a novel, syntaxin 13-interacting protein involved in platelet storage pool deficiency. *Nat. Genet.* 23:329–332. http://dx.doi.org/10.1038/15507

Downloaded from on October 24, 2016

Published August 1, 2016

Huizing, M., Y. Anikster, D.L. Fitzpatrick, A.B. Jeong, M. D'Souza, M. Rausche, J.R. Toro, M.I. Kaiser-Kupfer, J.G. White, and W.A. Gahl. 2001. Hermansky-Pudlak syndrome type 3 in Ashkenazi Jews and other non-Puerto Rican patients with hypopigmentation and platelet storage-pool deficiency. *Am. J. Hum. Genet.* 69:1022–1032. http://dx.doi.org/10.1086/324168

Jahn, R., and R.H. Scheller. 2006. SNAREs--engines for membrane fusion. *Nat. Rev. Mol. Cell Biol.* 7:631–643. http://dx.doi.org/10.1038/nrm2002

Jani, R.A., L.K. Purushothaman, S. Rani, P. Bergam, and S.R. Setty. 2015. STX13 regulates cargo delivery from recycling endosomes during melanosome biogenesis. *J. Cell Sci.* 128:3263–3276. http://dx.doi.org/10.1242/jcs.171165

Kent, H.M., P.R. Evans, I.B. Schäfer, S.R. Gray, C.M. Sanderson, J.P. Luzio, A.A. Peden, and D.J. Owen. 2012. Structural basis of the intracellular sorting of the SNARE VAMP7 by the AP3 adaptor complex. *Dev. Cell.* 22:979–988. http://dx.doi.org/10.1016/j.devcel.2012.01.018

Lane, P.W., and E.L. Green. 1967. Pale ear and light ear in the house mouse. Mimic mutations in linkage groups XII and XVII. *J. Hered.* 58:17–20.

Loftus, S.K., D.M. Larson, L.L. Baxter, A. Antonellis, Y. Chen, X. Wu, Y. Jiang, M. Bittner, J.A. Hammer III, and W.J. Pavan. 2002. Mutation of melanosome protein RAB38 in chocolate mice. *Proc. Natl. Acad. Sci. USA.* 99:4471–4476. http://dx.doi.org/10.1073/pnas.072087599

Lopes, V.S., C. Wasmeier, M.C. Seabra, and C.E. Futter. 2007. Melanosome maturation defect in Rab38-deficient retinal pigment epithelium results in instability of immature melanosomes during transient melanogenesis. *Mol. Biol. Cell.* 18:3914–3927. http://dx.doi.org/10.1091/mbc.E07-03-0268

Luzio, J.P., S.R. Gray, and N.A. Bright. 2010. Endosome-lysosome fusion. *Biochem. Soc. Trans.* 38:1413–1416. http://dx.doi.org/10.1042/BST0381413

Marks, M.S., H.F.G. Heijnen, and G. Raposo. 2013. Lysosome-related organelles: unusual compartments become mainstream. *Curr. Opin. Cell Biol.* 25:495–505. http://dx.doi.org/10.1016/j.ceb.2013.04.008

Martina, J.A., K. Moriyama, and J.S. Bonifacino. 2003. BLOC-3, a protein complex containing the Hermansky-Pudlak syndrome gene products HPS1 and HPS4. *J. Biol. Chem.* 278:29376–29384. http://dx.doi.org/10.1074/jbc.M301294200

Martinez-Arca, S., R. Rudge, M. Vacca, G. Raposo, J. Camonis, V. Proux-Gillardeaux, L. Daviet, E. Formstecher, A. Hamburger, F. Filippini, et al. 2003. A dual mechanism controlling the localization and function of exocytic v-SNAREs. *Proc. Natl. Acad. Sci. USA.* 100:9011–9016. http://dx.doi.org/10.1073/pnas.1431910100

McGough, I.J., F. Steinberg, M. Gallon, A. Yatsu, N. Ohbayashi, K.J. Heesom, M. Fukuda, and P.J. Cullen. 2014. Identification of molecular heterogeneity in SNX27-retromer-mediated endosome-to-plasma-membrane recycling. *J. Cell Sci.* 127:4940–4953. http://dx.doi.org/10.1242/jcs.156299

Meng, R., Y. Wang, Y. Yao, Z. Zhang, D.C. Harper, H.F.G. Heijnen, A. Sitaram, W. Li, G. Raposo, M.J. Weiss, et al. 2012. SLC35D3 delivery from megakaryocyte early endosomes is required for platelet dense granule biogenesis and is differentially defective in Hermansky-Pudlak syndrome models. *Blood.* 120:404–414. http://dx.doi.org/10.1182/blood-2011-11-389551

Mohrmann, R., H. de Wit, M. Verhage, E. Neher, and J.B. Sørensen. 2010. Fast vesicle fusion in living cells requires at least three SNARE complexes. *Science.* 330:502–505. http://dx.doi.org/10.1126/science.1193134

Molino, D., S. Nola, S.M. Lam, A. Verraes, V. Proux-Gillardeaux, G. Boncompain, F. Perez, M. Wenk, G. Shui, L. Danglot, and T. Galli. 2015. Role of tetanus neurotoxin insensitive vesicle-associated membrane protein in membrane domains transport and homeostasis. *Cell. Logist.* 5:e1025182. http://dx.doi.org/10.1080/21592799.2015.1025182

Morita, S., T. Kojima, and T. Kitamura. 2000. Plat-E: an efficient and stable system for transient packaging of retroviruses. *Gene Ther.* 7:1063–1066. http://dx.doi.org/10.1038/sj.gt.3301206

Nazarian, R., J.M. Falcón-Pérez, and E.C. Dell'Angelica. 2003. Biogenesis of lysosome-related organelles complex 3 (BLOC-3): a complex containing the Hermansky-Pudlak syndrome (HPS) proteins HPS1 and HPS4. *Proc. Natl. Acad. Sci. USA.* 100:8770–8775. http://dx.doi.org/10.1073/pnas.1532040100

Newell-Litwa, K., G. Salazar, Y. Smith, and V. Faundez. 2009. Roles of BLOC-1 and adaptor protein-3 complexes in cargo sorting to synaptic vesicles. *Mol. Biol. Cell.* 20:1441–1453. http://dx.doi.org/10.1091/mbc.E08-05-0456

Nguyen, T., and M.L. Wei. 2007. Hermansky-Pudlak HPS1/pale ear gene regulates epidermal and dermal melanocyte development. *J. Invest. Dermatol.* 127:421–428. http://dx.doi.org/10.1038/sj.jid.5700566

Nguyen, T., E.K. Novak, M. Kermani, J. Fluhr, L.L. Peters, R.T. Swank, and M.L. Wei. 2002. Melanosome morphologies in murine models of hermansky-pudlak syndrome reflect blocks in organelle development. *J. Invest. Dermatol.* 119:1156–1164. http://dx.doi.org/10.1046/j.1523-1747.2002.19535.x

Orlow, S.J., R.E. Boissy, D.J. Moran, and S. Pifko-Hirst. 1993. Subcellular distribution of tyrosinase and tyrosinase-related protein-1: implications for melanosomal biogenesis. *J. Invest. Dermatol.* 100:55–64. http://dx.doi.org/10.1111/1523-1747.ep12354138

Osanai, K., J. Higuchi, R. Oikawa, M. Kobayashi, K. Tsuchihara, M. Iguchi, J. Huang, D.R. Voelker, and H. Toga. 2010. Altered lung surfactant system in a Rab38-deficient rat model of Hermansky-Pudlak syndrome. *Am. J. Physiol. Lung Cell. Mol. Physiol.* 298:L243–L251. http://dx.doi.org/10.1152/ajplung.00242.2009

Prekeris, R., J. Klumperman, Y.A. Chen, and R.H. Scheller. 1998. Syntaxin 13 mediates cycling of plasma membrane proteins via tubulovesicular recycling endosomes. *J. Cell Biol.* 143:957–971. http://dx.doi.org/10.1083/jcb.143.4.957

Pryor, P.R., L. Jackson, S.R. Gray, M.A. Edeling, A. Thompson, C.M. Sanderson, P.R. Evans, D.J. Owen, and J.P. Luzio. 2008. Molecular basis for the sorting of the SNARE VAMP7 into endocytic clathrin-coated vesicles by the ArfGAP Hrb. *Cell.* 134:817–827. http://dx.doi.org/10.1016/j.cell.2008.07.023

Pu, J., C. Schindler, R. Jia, M. Jarnik, P. Backlund, and J.S. Bonifacino. 2015. BORC, a multisubunit complex that regulates lysosome positioning. *Dev. Cell.* 33:176–188. http://dx.doi.org/10.1016/j.devcel.2015.02.011

Richmond, B., M. Huizing, J. Knapp, A. Koshoffer, Y. Zhao, W.A. Gahl, and R.E. Boissy. 2005. Melanocytes derived from patients with Hermansky-Pudlak Syndrome types 1, 2, and 3 have distinct defects in cargo trafficking. *J. Invest. Dermatol.* 124:420–427. http://dx.doi.org/10.1111/j.0022-202X.2004.23585.x

Ryder, P.V., R. Vistein, A. Gokhale, M.N. Seaman, M.A. Puthenveedu, and V. Faundez. 2013. The WASH complex, an endosomal Arp2/3 activator, interacts with the Hermansky-Pudlak syndrome complex BLOC-1 and its cargo phosphatidylinositol-4-kinase type IIα. *Mol. Biol. Cell.* 24:2269–2284. http://dx.doi.org/10.1091/mbc.E13-02-0088

Salazar, G., B. Craige, M.L. Styers, K.A. Newell-Litwa, M.M. Doucette, B.H. Wainer, J.M. Falcon-Perez, E.C. Dell'Angelica, A.A. Peden, E. Werner, and V. Faundez. 2006. BLOC-1 complex deficiency alters the targeting of adaptor protein complex-3 cargoes. *Mol. Biol. Cell.* 17:4014–4026. http://dx.doi.org/10.1091/mbc.E06-02-0103

Schäfer, I.B., G.G. Hesketh, N.A. Bright, S.R. Gray, P.R. Pryor, P.R. Evans, J.P. Luzio, and D.J. Owen. 2012. The binding of Varp to VAMP7 traps VAMP7 in a closed, fusogenically inactive conformation. *Nat. Struct. Mol. Biol.* 19:1300–1309. http://dx.doi.org/10.1038/nsmb.2414

Setty, S.R.G., D. Tenza, S.T. Truschel, E. Chou, E.V. Sviderskaya, A.C. Theos, M.L. Lamoreux, S.M. Di Pietro, M. Starcevic, D.C. Bennett, et al. 2007. BLOC-1 is required for cargo-specific sorting from vacuolar early endosomes toward lysosome-related organelles. *Mol. Biol. Cell.* 18:768–780. http://dx.doi.org/10.1091/mbc.E06-12-1066

Setty, S.R.G., D. Tenza, E.V. Sviderskaya, D.C. Bennett, G. Raposo, and M.S. Marks. 2008. Cell-specific ATP7A transport sustains copper-dependent tyrosinase activity in melanosomes. *Nature.* 454:1142–1146. http://dx.doi.org/10.1038/nature07163

Seward, S.L. Jr., and W.A. Gahl. 2013. Hermansky-Pudlak syndrome: health care throughout life. *Pediatrics.* 132:153–160. http://dx.doi.org/10.1542/peds.2012-4003

Sitaram, A., and M.S. Marks. 2012. Mechanisms of protein delivery to melanosomes in pigment cells. *Physiology (Bethesda).* 27:85–99. http://dx.doi.org/10.1152/physiol.00043.2011

Sitaram, A., M.K. Dennis, R. Chaudhuri, W. De Jesus-Rojas, D. Tenza, S.R.G. Setty, C.S. Wood, E.V. Sviderskaya, D.C. Bennett, G. Raposo, et al. 2012. Differential recognition of a dileucine-based sorting signal by AP-1 and AP-3 reveals a requirement for both BLOC-1 and AP-3 in delivery of OCA2 to melanosomes. *Mol. Biol. Cell.* 23:3178–3192. http://dx.doi.org/10.1091/mbc.E11-06-0509

Suzuki, T., W. Li, Q. Zhang, A. Karim, E.K. Novak, E.V. Sviderskaya, S.P. Hill, D.C. Bennett, A.V. Levin, H.K. Nieuwenhuis, et al. 2002. Hermansky-Pudlak syndrome is caused by mutations in HPS4, the human homolog of the mouse light-ear gene. *Nat. Genet.* 30:321–324.

Sviderskaya, E.V., S.P. Hill, T.J. Evans-Whipp, L. Chin, S.J. Orlow, D.J. Easty, S.C. Cheong, D. Beach, R.A. DePinho, and D.C. Bennett. 2002. p16(Ink4a) in melanocyte senescence and differentiation. *J. Natl. Cancer Inst.* 94:446–454. http://dx.doi.org/10.1093/jnci/94.6.446

Takeuchi, S., Y. Abe, T. Yamada, S. Kawano, Y. Hozumi, S. Ito, T. Suzuki, and C. Nishigori. 2014. Case of Hermansky-Pudlak syndrome 1 patient with milder symptoms in Japanese. *J. Dermatol.* 41:268–270. http://dx.doi.org/10.1111/1346-8138.12390

Tamura, K., N. Ohbayashi, Y. Maruta, E. Kanno, T. Itoh, and M. Fukuda. 2009. Varp is a novel Rab32/38-binding protein that regulates Tyrp1 trafficking in melanocytes. *Mol. Biol. Cell.* 20:2900–2908. http://dx.doi.org/10.1091/mbc.E08-12-1161

Downloaded from on October 24, 2016

Published August 1, 2016

Tamura, K., N. Ohbayashi, K. Ishibashi, and M. Fukuda. 2011. Structure-function analysis of VPS9-ankyrin-repeat protein (Varp) in the trafficking of tyrosinase-related protein 1 in melanocytes. *J. Biol. Chem.* 286:7507–7521. http://dx.doi.org/10.1074/jbc.M110.191205

Theos, A.C., D. Tenza, J.A. Martina, I. Hurbain, A.A. Peden, E.V. Sviderskaya, A. Stewart, M.S. Robinson, D.C. Bennett, D.F. Cutler, et al. 2005. Functions of adaptor protein (AP)-3 and AP-1 in tyrosinase sorting from endosomes to melanosomes. *Mol. Biol. Cell.* 16:5356–5372. http://dx.doi.org/10.1091/mbc.E05-07-0626

Vijayasaradhi, S., Y. Xu, B. Bouchard, and A.N. Houghton. 1995. Intracellular sorting and targeting of melanosomal membrane proteins: identification of signals for sorting of the human brown locus protein, gp75. *J. Cell Biol.* 130:807–820. http://dx.doi.org/10.1083/jcb.130.4.807

Wade, N., N.J. Bryant, L.M. Connolly, R.J. Simpson, J.P. Luzio, R.C. Piper, and D.E. James. 2001. Syntaxin 7 complexes with mouse Vps10p tail interactor 1b, syntaxin 6, vesicle-associated membrane protein (VAMP)8, and VAMP7 in b16 melanoma cells. *J. Biol. Chem.* 276:19820–19827. http://dx.doi.org/10.1074/jbc.M010838200

Wang, F., H. Zhang, X. Zhang, Y. Wang, F. Ren, X. Zhang, Y. Zhai, and Z. Chang. 2008. Varp interacts with Rab38 and functions as its potential effector. *Biochem. Biophys. Res. Commun.* 372:162–167. http://dx.doi.org/10.1016/j.bbrc.2008.05.017

Wasmeier, C., M. Romao, L. Plowright, D.C. Bennett, G. Raposo, and M.C. Seabra. 2006. Rab38 and Rab32 control post-Golgi trafficking of melanogenic enzymes. *J. Cell Biol.* 175:271–281. http://dx.doi.org/10.1083/jcb.200606050

Wassmer, T., N. Attar, M. Harterink, J.R. van Weering, C.J. Traer, J. Oakley, B. Goud, D.J. Stephens, P. Verkade, H.C. Korswagen, and P.J. Cullen. 2009. The retromer coat complex coordinates endosomal sorting and dynein-mediated transport, with carrier recognition by the trans-Golgi network. *Dev. Cell.* 17:110–122. http://dx.doi.org/10.1016/j.devcel.2009.04.016

Wei, M.L. 2006. Hermansky-Pudlak syndrome: a disease of protein trafficking and organelle function. *Pigment Cell Res.* 19:19–42. http://dx.doi.org/10.1111/j.1600-0749.2005.00289.x

Wei, A.-H., and W. Li. 2013. Hermansky-Pudlak syndrome: pigmentary and non-pigmentary defects and their pathogenesis. *Pigment Cell Melanoma Res.* 26:176–192. http://dx.doi.org/10.1111/pcmr.12051

Yatsu, A., N. Ohbayashi, K. Tamura, and M. Fukuda. 2013. Syntaxin-3 is required for melanosomal localization of Tyrp1 in melanocytes. *J. Invest. Dermatol.* 133:2237–2246. http://dx.doi.org/10.1038/jid.2013.156

Zhang, X., X. He, X.Y. Fu, and Z. Chang. 2006. Varp is a Rab21 guanine nucleotide exchange factor and regulates endosome dynamics. *J. Cell Sci.* 119:1053–1062. http://dx.doi.org/10.1242/jcs.02810

Downloaded from on October 24, 2016